Nanoscale

REVIEW

View Article Online
View Journal | View Issue

Cite this: *Nanoscale*, 2025, **17**, 88

Two sides of the coin: synthesis and applications of Janus particles

Yifan Li,[a] Fei Liu,[a] Serkan Demirci,[a] Utsav Kumar Dey,[a] Thamer Rawah,[a] Aneeba Chaudary,[a] Ricardo Ortega,[a] Zhengtao Yang,[a] Emad Pirhadi,[b] Bingrui Huang,[a] Xin Yong[b] and Shan Jiang*[a,c]

Named after the two-faced Roman god, Janus particles (JPs) are defined by their distinct dual chemical compositions on a single particle. Research on micron-sized JPs has yielded remarkable insights, showcasing their unique assembly behaviors both in bulk and at interfaces. However, significant challenges persist, particularly in the synthesis of smaller (<500 nm) JPs, which remains complex and difficult to scale up. To date, there has been no commercial success with JPs. Recently, seeded synthesis methods, such as emulsion polymerization that is already employed in industrial-scale manufacturing, have shown great promise. These methods enable the production of high-quality JPs with different sizes, morphologies, and functionalities. This advancement has inspired more efforts in exploring JP applications across various fields, including emulsion stabilization, drug delivery, electronic devices, and coatings. This review provides a comprehensive overview of the recent progress in the synthesis and application of polymeric JPs, with an emphasis on the seeded synthesis approach. It discusses the underlying reaction mechanisms and explores different strategies for controlling JP morphology. Serving as a roadmap, this review aims to guide the design of novel functional JPs and their potential future applications. The successful implementation of JPs will require careful consideration and a deep understanding of both synthesis and applications, as these are indeed two sides of the same coin.

Received 6th September 2024,
Accepted 31st October 2024

DOI: 10.1039/d4nr03652b

rsc.li/nanoscale

[a]*Department of Materials Science and Engineering, Iowa State University of Science and Technology, Ames, IA 50011, USA. E-mail: sjiang1@iastate.edu*
[b]*Department of Mechanical and Aerospace Engineering, University at Buffalo, Buffalo, NY 14260, USA*
[c]*Division of Materials Science & Engineering, Ames National Laboratory, Ames, IA 50011, USA*

1. Introduction

The study of chemically anisotropic colloidal particles gained significant attention after P. G. de Gennes introduced the concept of Janus particles (JPs) in his 1991 Nobel lecture, "soft

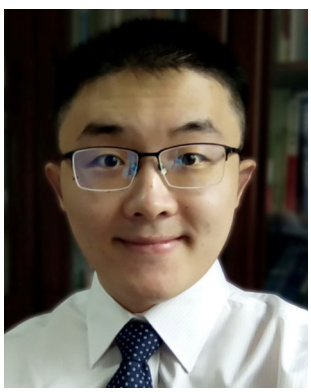

Yifan Li

Dr Yifan Li earned his Ph.D. and completed postdoctoral training at Iowa State University under Prof. Shan Jiang, focusing on Janus particles and coating applications. His research includes morphology control of polymeric Janus particles, emulsion polymerization, coating formulation, and nanoparticle self-assembly. He is also a co-inventor on several patents and actively engaged in the commercialization of his technologies.

Fei Liu

Dr Fei Liu is a research scientist in the Materials Science and Engineering Department at Iowa State University. He earned his Ph. D. from Peking University in 2015, specializing in the synthesis and application of magnetic nanocomposites. He joined Iowa State University as a postdoctoral researcher and later advanced to his current role as a research scientist. His broad research interests include the synthesis and assembly of Janus nanoparticles, electrocatalysis, and the development of conductive and semiconducting inks for additive manufacturing of electronic devices.

matter".[1] Named after the two-faced Roman god Janus, these particles are defined by their two distinct chemical compositions on either side.[2] With their asymmetric geometry mimicking small surfactant molecules, de Gennes speculated that JPs could be particularly useful in interface-related applications due to their strong adsorption at interfaces. Subsequent research has confirmed their unique assembly behaviors in both interfacial and bulk environments. For example, amphiphilic JPs can reside at the interface for extended periods, making them highly effective emulsifiers, while bipolar JPs form distinct cluster structures in bulk.[3,4] Additionally, amphiphilic JPs form intriguing crystal structures with long-range orientation correlations.[5] Many of these structures have been further predicted through theoretical models and computer simulations, providing a deeper fundamental understanding of JP interactions.[6–11]

JPs also offer the ability to combine multiple properties within a single particle, such as magnetic responsiveness and optical properties.[12,13] By imparting different functionalities to each hemisphere, these particles have found applications in catalysis,[14–21] sensing,[22–27] and drug delivery,[28–36] particularly with inorganic Janus nanocrystals, where multiple functionalities can be easily integrated.[37] Recent research has also explored the concept of "active particles", where JPs are modified to exhibit self-propulsion. This is achieved by designing one side of the particle to generate bubbles through reactions with "fuels" in the solution, enabling directed movement.[38–42] Alternatively, JPs can be directed using a magnetic field when integrated with magnetically responsive materials, or manipulated under an electric field through electrophoresis.[43–45] However, active particles have been reviewed elsewhere and are beyond the scope of this paper.

Despite tremendous progress in the research of micron-sized JPs, challenges remain in synthesizing JPs smaller than 500 nm.[46] Moreover, there has been no commercial success with JPs, despite numerous studies highlighting their potential in catalysis, emulsion stabilization, drug delivery, and separation.[47,48] The translation of fundamental knowledge into real-world applications has been elusive. Obviously, the cost of synthesizing JPs cannot outweigh their benefits. Furthermore, the applications of JPs are closely linked to their synthesis. For instance, magnetic amphiphilic JPs are required for oil–water separation applications, utilizing a magnetic field and the JPs' ability to adsorb at interfaces. Inorganic catalysts must be incorporated into JPs to leverage their catalytic properties. Similarly, drugs or diagnostic agents need to be integrated into JPs for theranostic applications. Therefore, synthesis and application are indeed two sides of the same coin. Reviewing recent progress in JP synthesis and application may offer insights into future directions for the field.

JPs can be categorized into three main types: inorganic–inorganic, polymer–polymer, and organic–inorganic hybrid particles.[49] These particles exhibit a variety of shapes and structures, including spherical and non-spherical forms such as dumbbell, acorn, and snowman-like configurations.[50,51] A promising scalable fabrication strategy for creating these asymmetric structures is seeded growth, which leverages phase separation and selective surface modification.[52–56] This review focuses particularly on seeded emulsion polymerization, highlighting it as a cost-effective approach for achieving a large quantity of high-quality JPs with the desired morphology and functionality. In addition, emulsion polymerization uses water as the primary solvent, making it a more environmentally friendly process compared with other polymerization techniques. This feature makes the process more favorable for industrial scale-up, as it reduces the use of harmful organic solvents and decreases volatile organic compound (VOC) emissions. However, the polymerization process is influenced by many factors such as surface tension, solvent composition, and monomer selection, often requiring an extensive trial-and-error approach.[57] Integrating theoretical calculations and simulations with experimental data can significantly enhance the design and optimization of particle synthesis. As outlined in Fig. 1, we first overview the examples of JPs synthesis, examining key strategies for controlling particle morphology, including seed chemistry, crosslinking, the selection of sec-

Serkan Demirci

Dr Serkan Demirci is an Associate Professor at Amasya University, Türkiye. Currently, he is working as a visiting professor at Iowa State University. He obtained his Ph.D. at Gazi University, focusing on polymer brushes, and completed postdoctoral research at Bilkent University-UNAM on electrospun nanofibers and applications. His research focuses on developing functional polymers and advanced polymeric materials for a sustainable and green future.

Utsav Kumar Dey

Utsav Kumar Dey earned his M. S. in Inorganic Chemistry from Iowa State University in 2021 and is currently a Ph.D. candidate in Materials Science and Engineering under the guidance of Dr Shan Jiang. His research focuses on the design and synthesis of Janus nanoparticles using emulsion polymerization techniques to develop multifunctional coatings.

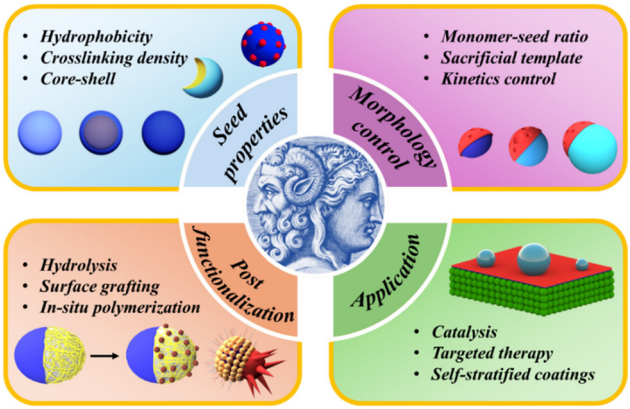

Fig. 1 Schematic illustration of the synthetic methods that influence the morphology and functionality of JPs.

ondary monomers, and post-functionalization techniques. Then we discuss the diverse applications of JPs across various fields, emphasizing how synthesis methods and particle composition influence performance. Finally, we offer a perspective on future directions, addressing the challenges and potential advancements that could drive the next phase of research and development in this area.

2. Synthesis method

Several methods have been developed for fabricating JPs, including protection-release,[4,5,58–64] seeded growth,[54,65–68] microfluidics,[69–74] and block copolymer-derived approaches.[75–82] These methods generally fall into two categories: top-down and bottom-up as summarized in Table 1. The top-down approach modifies existing particles through protection-release mechanisms, while the bottom-up approach builds particles from scratch. Seeded synthesis is a key technique in the bottom-up fabrication of JPs, utilizing preformed seed particles as nucleation sites for the growth of Janus structures. This process begins with the synthesis of seed particles, which can be composed of either organic or inorganic materials. These seed particles provide a starting point, ensuring uniformity in the size and shape of the resulting JPs. The characteristic Janus morphology typically arises from phase separation at the single-particle level.

Both top-down and bottom-up approaches can produce particles with varying sizes, morphologies, and chemical compositions, but each method has its own advantages and limitations. For instance, one top-down method involves directional coating of a monolayer of particles on a flat substrate, resulting in well-defined Janus morphologies; however, this technique is limited to micron-sized particles and yields only small quantities per batch (1–10 mg).[60] While these particles serve as excellent model systems for fundamental studies, the method is challenging to scale up and unsuitable for large-scale applications. In contrast, bottom-up approaches are more scalable but can be more difficult to control. In this review, we focus on the bottom-up approach and discuss three types of JP: inorganic, polymeric, and hybrid. Although these nanoparticles are diverse, their seeded synthesis processes share common features and principles, which we will first overview before exploring each type of JP in detail.

The first critical factor to consider in seeded synthesis is the properties of the seed particles. These properties are crucial for achieving the desired Janus morphology, as they dictate phase separation and influence the subsequent growth phase. When monomers or precursors are added to the system and undergo polymerization or other chemical reactions invol-

Xin Yong

Dr Xin Yong is currently an Associate Professor in the Department of Mechanical and Aerospace Engineering at the University at Buffalo (UB). He received his BS degree in physics at Peking University in 2007 and PhD degree in mechanical engineering from Rensselaer Polytechnic Institute in 2012. Prior to joining UB, he conducted postdoctoral research at the University of Pittsburgh and held the positions of Assistant Professor and Associate Professor at Binghamton University. Dr Yong's research employs multiscale approaches for simulating and modeling fluid dynamics and transport phenomena in soft and active matter, focusing on emergent interfacial behaviors in these systems.

Shan Jiang

Dr Shan Jiang is an Associate Professor in the Materials Science and Engineering department at Iowa State University. He earned his Ph.D. at the University of Illinois at Urbana-Champaign under Prof. Steve Granick, focusing on Janus particles, and completed postdoctoral research at MIT's Langer Lab on gene delivery for cancer therapy. Prior to academia, he worked as a research scientist at Dow Chemical in coating materials. His research spans Janus particles, biomaterials, additive manufacturing, and plant gene editing. Dr Jiang is also actively involved in efforts to commercialize technologies developed in his lab.

Table 1 Summary of different methods of synthesizing JPs

Method	Category	Chemistry	Size	Morphology	Scalability
Direct deposition	Top-down	Organic and inorganic	1 μm–10 μm	Sphere, rod	No
Emulsion polymerization	Bottom-up	Organic	50 nm–5 μm	Dumbbell, sphere, multi-lobe	Yes
Nanocrystal growth	Bottom-up	Inorganic	5 nm–100 nm	Dumbbell	Yes
Microfluid	Bottom-up	Organic	1 μm–100 μm	Sphere	Moderate
Block copolymer	Bottom-up	Organic	5 nm–50 nm	Sphere, rod	Yes

ving the seed particles, the intrinsic incompatibility between the seed and secondary monomers drives phase separation. This process leads to the formation of distinct separated phases within the particle, with unique chemical compositions and properties.[83,84] Factors such as temperature, solvent choice, and the presence of surfactants or stabilizers further influence this separation, resulting in particles with specific morphologies.[3,12,53] We will first explore seeded nanocrystal growth for the formation of inorganic JPs and then discuss emulsion polymerization for creating organic polymeric JPs. Although these two methods differ significantly, it is valuable to examine their common principles. On the other hand, we will not provide a comprehensive account of all methods. For example, the wax emulsion method produces JPs by selectively modifying the exposed surface of particles trapped at the wax droplet surface, and the microfluidic approach by using photopolymerization that enables the formation of JPs.[85,86] These methods have their own merits but are out of the scope of this review. The key point is that each method offers unique advantages, making it essential to select the appropriate technique based on the desired chemistry, size, morphology, and application. In the morphology control section, we will showcase successful examples of JP synthesis and discuss key principles derived from these various methods.

2.1. Seeded nanocrystal growth for inorganic JPs

Inorganic JPs have attracted significant attention due to their ability to combine multiple functionalities within a single material platform.[87] The intrinsic properties, such as plasmonic, magnetic, and fluorescent characteristics, enable the breakthroughs in various applications, including catalysis, sensing, diagnosis, and therapy.[88,89] Moreover, the interactions between two functional components across their interface often bring various interesting synergistic effects, leading to enhanced performance in various applications. While several reviews have summarized the efforts in this area, we will highlight more recent developments, focusing specifically on amphiphilic Janus nanocrystals, also known as "nanosurfactants".[90–93]

The seed-mediated approach has proved particularly effective for synthesizing inorganic JPs, offering precise control over size, geometry, and architecture.[94] This process follows the principles of heterogeneous nucleation and subsequent growth, where the lattice mismatch between different components plays a critical role. This mismatch determines the interfacial energy between the components, leading to the formation of core–shell or dumbbell-like structures. Factors such as reaction temperature, surfactant choice, precursor materials, and solvent selection are crucial in controlling the final geometry of the JPs. Typically, homogeneous nanoparticles are first synthesized and then used as seeds. When a second component is added, the high surface energy of the preformed seeds in solution promotes nucleation on their surface, thereby inhibiting the homogeneous nucleation of separate nanoparticles. A variety of materials, including metals, oxides, and chalcogenides, can serve as seeds, although metal nanoparticles are most commonly used due to their suitability for enabling the heterogeneous nucleation of a secondary component. Consequently, the construction of various inorganic JPs, such as metal–metal, metal–oxide, and metal–chalcogenide, has been extensively studied.

One notable example for seeded nanocrystal growth is the synthesis of Au–Fe_3O_4 inorganic JPs, where dumbbell-like Au–Fe_3O_4 nanoparticles are used as core materials and their surfaces are modified carefully to produce the amphiphilicity (Fig. 2a and b).[95] The process begins with the formation of Au seed nanoparticles, followed by a secondary growth step that forms an Fe_3O_4 lobe through a high temperature-triggered reaction approach. The ratio of oleylamine and oleic acid is carefully controlled to favor the formation of a dumbbell-like geometry rather than core–shell structures. High-resolution TEM images of typical Au–Fe_3O_4 nanoparticles clearly indicate the heteroepitaxial growth of Fe_3O_4 onto Au, resulting in a dumbbell-like morphology. However, the as-synthesized Au–Fe_3O_4 nanoparticles are chemically homogenous, as both the Au and Fe_3O_4 surfaces are coated with oleylamine and oleic acid, making the nanoparticles highly oleophilic and incompatible with aqueous solutions. Advances in surface modification techniques allow for the modification of the Au and Fe_3O_4 surfaces with hydrophilic and hydrophobic ligands through a ligand exchange process, rendering the nanoparticles amphiphilic.[96,97] Typically, Au–S chemistry is employed to protect the Au lobe with thiols (*e.g.*, 1-octadecanethiol) to maintain its hydrophobicity, while Fe_3O_4 is modified with 3,4-dihydroxybenzoic acid *via* a metallocyclic chelate, providing the necessary charge to stabilize the particles in aqueous solution. An acid treatment step is also crucial for cleaning the Au surface, enhancing the amphiphilicity of the Janus Au–Fe_3O_4 nanoparticles. These amphiphilic nanoparticles behave like molecular surfactants, effectively reducing water–oil interfacial tension and self-assembling into micelle-like nanostructures in aqueous solution. Notably, their amphiphilicity can be

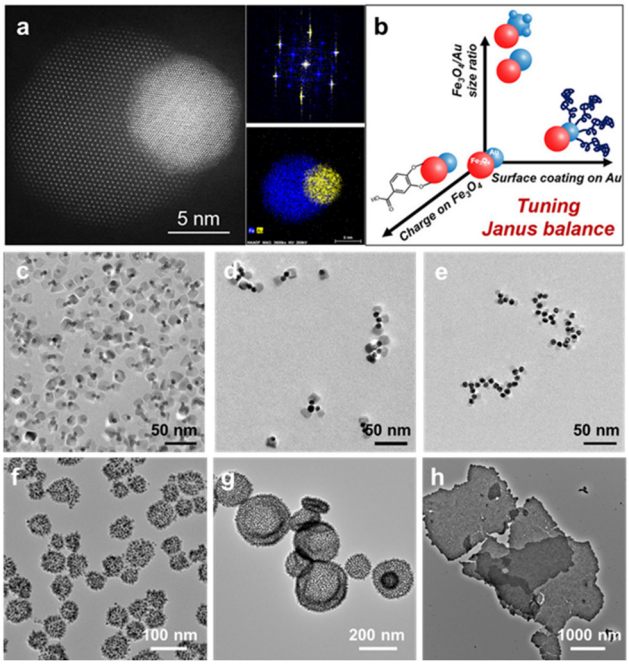

Fig. 2 (a) HAADF-STEM image of a typical Au–Fe_3O_4 nanocrystal and its corresponding fast FFT patterns and EDS elemental mapping. (b) Strategies for tuning of the Janus balance of Au–Fe_3O_4 nanocrystals. (c–h) Self-assembly structures of Au–Fe_3O_4 nanocrystals, including clusters, chains, micelles, capsules, and sheets. Reproduced from ref. 95 with permission from the American Chemical Society. Copyright 2019.

finely tuned by adjusting the "Janus balance", which can be simply defined as the ratio of radii between the Au and Fe_3O_4 lobes and is analogous to the hydrophilic–lipophilic balance (HLB) in molecular surfactants. The Au lobe can be further enlarged through an additional growth step, with Au–Fe_3O_4 nanoparticles serving as seeds, ensuring that Au deposition occurs only on the Au lobe in the JP.

These strategies for controlling the Janus balance in amphiphilic Au–Fe_3O_4 nanoparticles not only enable their self-assembly into various structures—ranging from clusters and capsules to sheets and vesicles (Fig. 2c–h)—but also open up new possibilities in interfacial catalysis and biomedicine. Similar approaches have been used to synthesize other amphiphilic inorganic JPs, such as Au–Fe_3O_4 branched nanoparticles,[98] Au–PbS dimers,[96] and Ag_2S–CdS nanomatchsticks.[99]

2.2. Polymeric JPs obtained using seeded emulsion polymerization

Synthesis of polymeric JPs can be achieved through seeded emulsion polymerization. While the basic principle of growing Janus structures using seed particles and a secondary monomer is similar to that of inorganic Janus nanoparticle synthesis, key differences arise due to the nature of the polymeric system. In this case, the secondary monomer not only adsorbs onto the surface of the seed particles but also diffuses into the polymeric seed, leading to particle swelling and the formation of a more complex system. Initially, seed particles are synthesized through traditional polymerization methods such as emulsion or dispersion polymerization. When these seed particles are exposed to a second monomer, they swell as the monomer diffuses into them. As the concentration of the second monomer increases, phase separation occurs at the single-particle level, potentially leading to the formation of various final particle morphologies.[100]

2.2.1. Thermodynamic analysis. Thermodynamically, the development of particle morphology during seeded emulsion polymerization involves the diffusion of molecular species driven by Gibbs free energy changes, leading to a specific configuration. The calculation of Gibbs free energy helps predict whether the morphology will occur spontaneously. The thermodynamic analysis focuses on identifying the equilibrium configuration with the lowest free energy. This analysis does not consider the effect of resistance to molecular or polymer diffusion (*e.g.*, internal particle viscosity). Early studies on predicting multiphase particle morphology were based on the interfacial behavior of a three-phase fluid system, where two immiscible liquid droplets (phases 1 and 2) are suspended in a third immiscible liquid (phase 3). Torza and Mason showed that the interfacial tensions and spreading coefficients of the three phases determine the equilibrium configurations of droplet coalescence, including core–shell and hemispherical morphologies.[101] Several groups applied this approach to predict the phase separation and resulting surface morphology in composite polymer particles.[102–104] In these studies, the initial state of the system is considered to consist of a pure polymer phase (seed particles of polymer 1) suspended in water (possibly with surfactants) and a completely separated bulk phase of pure polymer 2 (postformed polymer). Assuming no phase changes, mixing or demixing is involved, and the only contribution to the free energy change is that of the creation of new interfaces between polymer 1/water, polymer 2/water, and polymer 1/polymer 2. The total free energy change can then be expressed as $\Delta G = \sum \gamma_{ij} A_{ij} - \gamma_{1w} A_0$ where γ_{ij} is the interfacial tension between the i and j phases and A_{ij} is the corresponding interfacial area depending on the particle morphology (Fig. 3). A_0 is the interfacial area of original polymer 1 particle suspended in water. Previous models are applicable only at the end of the latex production process. Chen *et al.* then extended the analysis to account for the extent of conversion of the seeded polymerization, during which the volume ratio of polymer 2 to polymer 1 changes.[105] The initial state of the thermodynamic model was revised to have polymer phase 1 represent seed particles of polymer 1 swollen by monomer 2 (Fig. 3). As a result, the expressions of free energy change depend on additional parameters like polymer/monomer densities, weight ratio of monomer 2 to polymer 1, and polymerization conversion. Using the revised model, Chen *et al.* investigated the influence of interfacial tension reduction in the presence of different surfactants on the particle morphology development. Several similar models were developed in parallel to include conversion-dependent pathways and predict the particle morphology as a function of

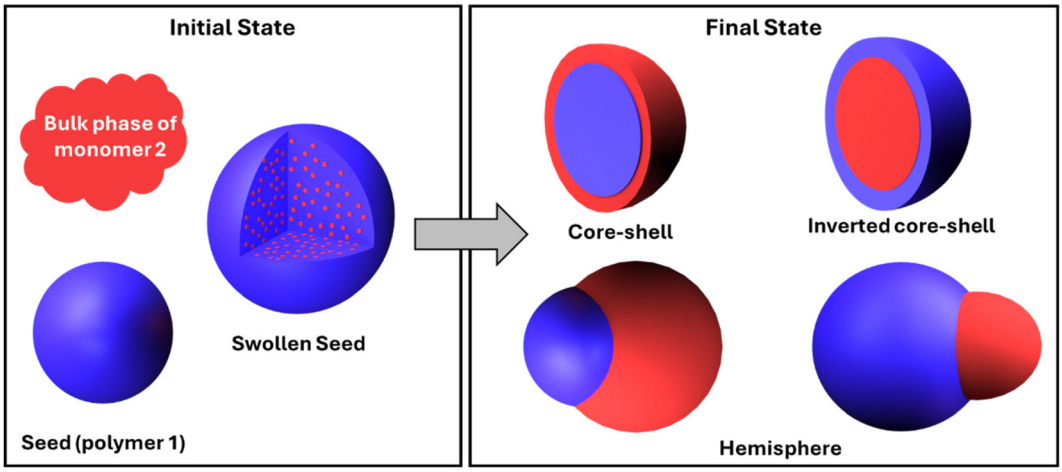

Fig. 3 Schematics of initial (reference) and final states for the interfacial tension-based thermodynamic analysis of morphology development in composite polymer particles.

the polymerization conversion.[106–108] Despite some success in predicting morphologies observed in the experiments, these models cannot fully capture all structures observed experimentally, and have significant limitations as they consider only interfacial tension and interface geometry. In particular, the solid nature of seed particles and the interactions between the seed and secondary monomer/polymer were not considered.

Sheu *et al.* independently developed a different thermodynamic model to account for the mixing of monomer 2 with crosslinked seed particles and induced seed swelling.[109] This new model explains that the phase separation, leading to anisotropic particle formation, is driven by the balance between the free energy of mixing of the monomer and seed polymer, the elastic energy of the crosslinked polymer network, and interfacial tension between the particle and the solvent continuous phase. The model can be expressed by the equation: $\Delta G_{m,p} = \Delta G_{el} + \Delta G_m + \Delta G_t$, where $\Delta G_{m,p}$ represents the total free energy change of the monomer in the particle phase. Here, ΔG_{el} denotes the change in elastic energy due to the seed network swelling, ΔG_m indicates the free energy change from the mixing of the monomer and polymer seed (determined by Flory–Huggins parameters), and ΔG_t refers to the change in interfacial surface energy between the particle and the solvent. The detailed expressions of ΔG_{el}, ΔG_m, and ΔG_t are given by the Flory–Huggins theory, Flory–Rehner equation, and Morton equation, respectively. When seed particles are at swelling equilibrium, the free energy of the monomer in the particle phase $\Delta G_{m,p}$ is equal to the free energy of the monomer in the solvent $\Delta G_{m,s}$. For monomers with low solubility in the solvent (*e.g.* styrene in water), the free energy of monomer in water is negligible, giving the swelling equation $\Delta G_{el} + \Delta G_m + \Delta G_t = 0$. The regime with $\Delta G_{m,p} > 0$ represents an unstable region in which the polymer network would spontaneously exude monomer to induce phase separation. This study argued that the phase separation of the swollen network is a viscoelastic process, which is induced by the relaxation of the polymer chains as a result of increasing temperature or longer swelling time.

Mock *et al.* applied Sheu's model in the synthesis of anisotropic nanoparticles *via* seeded emulsion polymerization.[100] They developed a multistep process where cross-linked polystyrene seed particles are first coated with a hydrophilic polymer layer. This coating increases the interfacial tension between the seed particle and the monomer and promotes the extent and uniformity of the anisotropy of the final particles. Kinetic factors, such as the rate of monomer diffusion and polymerization, also play a crucial role in developing the final particle morphology. Wei *et al.* produced anisotropic particles through the swelling of semi-interpenetrating network seed particles using photoinitiated polymerization, allowing swelling and polymerization to take place at room temperature. The results suggested that the critical condition is the swelling of semi-interpenetrating network seeds with a monomer, during which the phase separation is mainly driven by the entropy gain of linear polymer chains leaving the swollen seed.[110] In contrast to Sheu *et al.*, the temperature-induced recovery of the elastic network during the final polymerization is not a major contribution to anisotropy particle formation.

Next we turn our attention to systems involving different polymers, including polystyrene (PS), poly(tetradecyl acrylate) (PTA), polyethylenimine (PEI), polyvinyl acetate (PVAc), *tert*-butyl acrylate (*t*BA), propargyl acrylate (PA), 3-mercaptopropionic acid (MPA), 2-mercaptoethanol (MPE), cysteamine (CYA), polyacrylonitrile (PAN), 3-(triethoxysilyl)propyl-methacrylate (TPM), polypyrrole (PPy), and trimethoxysilyl-propane-1-thiol (TMPT).

2.2.2. Amphiphilic PS/PTA JPs. Kim *et al.* have made significant strides in synthesizing JPs.[57,111] Recognizing the challenge of swelling hydrophobic monomers into hydrophilic seeds, they addressed the issue by rendering the surface of PS-*co*-PVAc seed particles highly hydrophilic through saponifica-

tion, while maintaining a hydrophobic PS core. They then conducted a systematic study of various hydrophobic monomers with differing carbon chain lengths. Their results revealed that tetradecyl acrylate, with its 14-carbon chain, successfully swelled into these core–shell seeds, enabling the formation of distinct Janus morphologies. By adjusting the PS to PVAc ratio in the seed composition, they could further fine-tune the surface hydrophilicity, which in turn influenced the contact angles and particle morphology.

Moreover, by incorporating magnetic nanoparticles and utilizing photopolymerization, they produced JPs with magnetic responsiveness. Their theoretical calculations underscored the critical role of surface tension in predicting final particle shapes and understanding phase behavior. The resulting phase diagram provided an overview of the conditions necessary for achieving Janus morphologies, highlighting the importance of monomer swelling ratios and solvent composition. This comprehensive approach has significantly advanced the design and production of JPs with tailored functionalities, particularly for applications in stabilizing Pickering emulsions.

2.2.3. pH-Responsive JPs. By incorporating functional groups that can alter their properties in response to external stimuli or environmental changes, JPs can be transformed into smart materials. Tu *et al.* achieved the synthesis of pH-responsive JPs using a combination of seeded emulsion polymerization and polymerization-induced phase separation.[112] These particles have a unique composition, with one side rich in hydrophobic styrene and the other in pH-sensitive acrylic acid. Beginning with monodisperse linear polystyrene seeds, the researchers used a mixture of styrene and *t*BA as the secondary monomer. During copolymerization, styrene initially predominates, but as the reaction progresses, the increasing *t*BA concentration triggers polymerization-induced phase separation due to the high Flory–Huggins interaction parameter between styrene and *t*BA. Hydrolysis of the *t*BA units forms acidic groups, resulting in significant morphological changes, with particles transitioning from spherical to acorn-shaped or dumbbell-like structures. These JPs not only change shape but also reverse their amphiphilicity in response to pH changes. The study emphasizes the critical role of controlling the styrene-to-*t*BA ratio and hydrolysis to tailor pH responsiveness and shape transformations, offering valuable insights into the design of functional colloids with customized interfacial properties.

2.2.4. PAN/PS JPs. Tang *et al.* developed a method for synthesizing JPs composed of PAN and PS, achieving distinct separation between the two polymers on the particle surface.[52] The process involved the slow, dropwise addition of a styrene monomer and crosslinker DVB mixture to a cross-linked PAN seed, facilitating the phase separation required to form the Janus morphology. A crucial factor in the success of this method was the cross-linking of the PS shell, which ensured that the PS phase remained distinct and did not mix with the PAN seed, resulting in well-defined JPs. The study also demonstrated that by controlling the degree of cross-linking and the monomer feed rate, the size and morphology of the JPs could be precisely tuned.

2.2.5. Moon-shaped JPs. Fan *et al.* investigated the synthesis of JP through an emulsion interfacial polymerization approach, focusing on the critical role of non-crosslinked PS particles in controlling the reaction mechanism.[113,114] Their study revealed that when PS particles are preloaded into oil droplets containing a styrene and DVB monomer mixture, they dissolve to form free PS chains that significantly influence the polymerization process. These PS chains preferentially interact with the newly formed poly(styrene-divinylbenzene) (PS-PDVB) nuclei within the droplets. This interaction causes the PS chains to cover the PS-DVB nuclei, shielding some reactive sites from further polymerization. As the PS-DVB nuclei migrate toward the oil–water interface, the PS chains on the side facing the water phase re-expose these reactive sites, accelerating polymerization at the interface while slowing it within the droplet due to continued shielding. This differential polymerization rate results in the preferential growth of particles at the oil–water interface, leading to the formation of asymmetrical JPs. The study also demonstrated that by varying the concentration of PS polymer and monomers, the degree of shielding can be controlled, allowing fine-tuning of particle morphology to achieve diverse shapes, from hemispherical to crescent-moon. Theoretical simulations supported these findings, showing how PS chains modulate polymerization dynamics by controlling the exposure and shielding of reactive sites, ultimately dictating the topology and uniformity of the JPs.

2.3. Hybrid JPs obtained through seeded growth

Organic–inorganic hybrid JPs can be synthesized through modified seeded emulsion polymerization, where the inorganic component is introduced by using inorganic particles as seeds or by utilizing silane chemistry during the polymerization.[115] Similar principles of emulsion polymerization still apply, but additional considerations must account for the compatibility of inorganic particles. When silanes are involved, reaction conditions and kinetics differ from acrylate chemistry. Silanes are more reactive and sensitive to moisture, so emulsions are typically cooled with ice water to maintain reactivity before being added to the reaction. Since no single method works universally, each reaction requires careful optimization of specific conditions, such as temperature, pH, and reactant concentrations, to accommodate the reactivity of the involved materials.

Reculusa *et al.* synthesized hybrid organic–inorganic JPs through a seeded emulsion polymerization process, using surface-modified silica particles as seeds for the polymerization of styrene.[115] By adjusting the silica-to-monomer ratio and surface properties of the silica seeds, they controlled the final hybrid nanoparticle morphology, achieving shapes like dumbbells. This is one of the simplest approaches for incorporating inorganic particles into polymers *via* emulsion polymerization. The key to success lies in ensuring the compatibility of the inorganic particles with the emulsion system. This involves carefully selecting surfactants, stabilizers, and reaction conditions to maintain a stable emulsion while incorporating inorganic materials, ensuring proper dispersion, and avoiding agglomeration.

Xia *et al.* introduced metal–polymer hybrid seeds, using metal nanoparticles that served as templates to grow polymeric JPs with unique optical and catalytic properties.[116,117] These hybrid JPs combine the advantages of both organic and inorganic materials, making them versatile for a wide range of applications. The reaction mechanism involves PS oligomers nucleating and growing asymmetrically on the surface of the metal nanoparticles. Controlling phase separation and time of addition is critical to the success of this method.

Mihali *et al.* developed semiconductive JPs with tunable electrical resistance and surface polarity by asymmetrically functionalizing snowman-shaped JPs.[118] These particles featured one lobe made of semiconductive polypyrrole (PPy) and another composed of an electrically insulating silane-containing monomer, poly(3-triethoxysilylpropyl methacrylate) (P(3-TSPM)). The PPy lobe is selectively grown on one hemisphere of the particle through oxidative polymerization in the presence of an oxidizing agent, such as ammonium persulfate. This selective growth is influenced by the different surface charges of the two lobes at low pH, where the PPy preferentially attaches to the negatively charged PS lobe while avoiding the P(3-TSPM) lobe. By varying the relative size of the two lobes, the researchers could finely control the conductivity, achieving an order-of-magnitude change in bulk powder conductivity.

Rahman *et al.* developed anisotropic Janus-like magnetic microparticles using seed emulsion polymerization, with the choice of initiator, AIBN *versus* KPS, significantly affecting the final particle morphology.[119] AIBN, an oil-soluble initiator, promoted pronounced phase separation between the polystyrene and magnetic domains, leading to well-defined Janus structures. Conversely, KPS, a water-soluble initiator, resulted in more uniform particles with less distinct phase separation due to greater phase mixing during polymerization. Ge *et al.* synthesized superparamagnetic composite colloids with anisotropic structures using a multi-step process involving core–shell polymer-coated Fe_3O_4@SiO_2 particles as seeds and subsequent emulsion polymerization with styrene monomer.[120] The degree of phase separation and final particle morphology were controlled by adjusting the interfacial tension and crosslinker (DVB) concentration.

In summary, these hybrid particles combine the distinct properties of organic polymers and inorganic materials, resulting in enhanced structural integrity, tunable surface chemistries, and multifunctional capabilities. Techniques such as nanoparticle grafting, acid hydrolysis, and *in situ* surface polymerization further enhance their versatility, enabling applications ranging from drug delivery and catalysis to electronics and sensor technologies.

3. Morphology control

Morphology is critical to the behaviors and properties of JPs. Depending on the size, geometry, and relative position of the two sides, JPs can adopt various geometries, such as simple spherical shapes, dumbbells, snowmen, or even multilobe and raspberry-like structures. The morphology of JPs is influenced by several factors, including the monomer-to-seed ratio, seed properties (such as surface hydrophobicity and crosslinking density), properties of the second monomer, reaction kinetics, and solvent composition. Surface hydrophobicity plays a significant role in phase separation, as differences in surface energy drive the formation of distinct domains. Crosslinking density affects the rigidity of the particles, influencing the extent of swelling, phase separation, and resulting morphology. Additionally, factors like temperature, solvent choice, and the presence of surfactants or stabilizers can further impact morphology by affecting the kinetics and thermodynamics of the phase separation process. The interaction of these factors creates a complex landscape for morphological changes, making it essential to understand how they correlate. By understanding these principles, one can strategically use different approaches, such as surface modification, crosslinking, reaction conditions, solvent composition, and surfactant selection, to collectively control the final shape, size, and functionality of the particles.[121]

3.1. Seed properties

The selection of seed materials in the synthesis of polymeric JPs is a critical step that defines the initial template or core on which the Janus structure will be formed. This choice significantly influences the overall morphology, functionality, and stability of the resulting particles. Factors such as the desired shape, size, surface chemistry, and crosslinking density must be carefully considered. For example, the seed's surface chemistry plays a crucial role in incorporating second monomers and enabling subsequent surface modifications. Once the seed is formed, the second monomer is selected based on its ability to swell and phase-separate on the seed particles, allowing for the introduction of specific functionalities, such as hydrophobicity or catalytic activity.

3.1.1. Hydrophobicity. A common hydrophilic monomer, acrylic acid (AA), introduces hydrophilicity and a negatively charged surface to JPs due to its carboxylic acid groups. These functional groups ionize easily in water, making the particles highly hydrophilic and well-suited for interacting with aqueous environments. Such properties are particularly beneficial for applications in biological systems, such as drug delivery, where particles must be water-dispersible and compatible with biological molecules. In a study by Fan *et al.*, hybrid JPs were synthesized using a novel emulsion interfacial polymerization approach, with AA playing a critical role.[113,114] The process began with the creation of a polystyrene (PS) seed particle emulsion, which was then swollen with a mixture of styrene, DVB and AA. As shown in Fig. 4, the inclusion of AA was essential for introducing hydrophilic functional groups, which facilitated phase separation during polymerization. The initial polymerization of hydrophobic monomers inside the droplet could produce a particle nucleus that moved toward the oil/water interface. The hydrophilic anchoring monomers in the external water phase could contact the particle nucleus

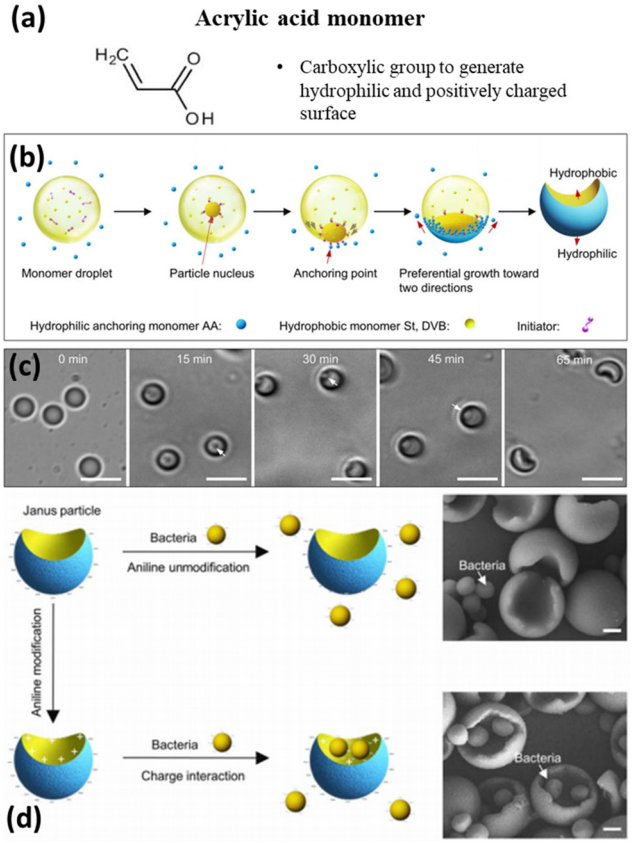

Fig. 4 Monomer selection – AA and emulsion interfacial polymerization mechanism for producing JPs. (a) Molecular structure of the acrylic acid monomer. (b) Schematic of the fabrication of JPs. (c) Bright-field microscope images of the time-dependent growth process of JPs. Scale bar, 5 μm. (d) Selective functionalization of the concave surface of JPs. JPs were used to capture and recognize spherical PS particles and live bacteria (*S. aureus*). Scale bar, 500 nm. Reproduced from ref. 113 with permission from the American Association for the Advancement of Science. Copyright 2017.

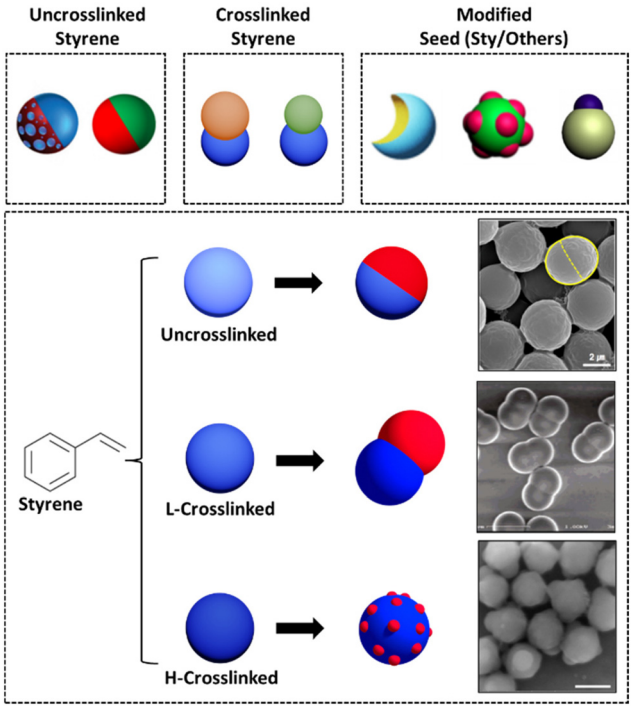

Fig. 5 Illustration of seed crosslinking and modification strategies for generating JPs with different morphologies. Uncrosslinked seeds typically result in spherical Janus particle morphologies, whereas crosslinked seeds often produce dumbbell-shaped JPs. A variety of morphologies can be achieved by modifying the seed structures. Representative SEM images corresponding to each seed type are attached. Reproduced from ref. 123 with permission from the American Chemical Society. Copyright 2006. Reproduced from ref. 124 with permission from Elsevier. Copyright 2019.

and be initiated to polymerize, thereby anchoring the particle at the interface of the droplet, triggering interfacial anchoring polymerization. Subsequently, based on the equal chemical potential principle at equilibrium, preferential copolymerization of AA, St, and DVB occurred along the interface in two directions, resulting in the formation of crescent moon-shaped JPs. As a result, the polymerization process, mediated by the PS seeds, produce JPs with distinct hydrophobic and hydrophilic domains.

Styrene is one of the most common hydrophobic monomers. To achieve an even higher degree of hydrophobicity, monomers that contain long carbon tails such as TA (tetradecyl acrylate) can be utilized. This makes it suitable for applications where water repellence is desired, such as in the creation of waterproof coatings. Kim[57,111] *et al.* and Li[122] *et al.* utilized tetradecyl acrylate to achieve hydrophobic surfaces in JPs, enhancing their hydrophobic properties in various applications.

3.1.2. Seed crosslinking density. Different types of seed and the resulting particle shapes achieved through various polymerization processes are illustrated in Fig. 5. Uncrosslinked styrene seeds typically produce spherical particles, while crosslinked styrene seeds can create dumbbell and raspberry-shaped particles depending on the monomer selection and feeding ratio. Modified seeds enable the formation of concave, raspberry, and snowman-shaped particles with distinct functional domains. These versatile templates provide a robust platform for developing advanced JPs with specific properties.

Uncrosslinked seeds are widely used as versatile templates for creating various Janus particle configurations due to their ability to swell with different monomers across a wide range of concentrations. Bradley[125] *et al.* demonstrated that uncrosslinked polystyrene (PS) seeds allowed for precise control over particle morphology during surfactant-free emulsion polymerization, leading to structures such as patchy-Janus and smooth spheres. Similarly, Kim *et al.* synthesized bi-compartmentalized amphiphilic Janus microparticles using uncrosslinked PS seeds, which uniformly swelled and polymerized to form well-defined Janus structures without the rigidity imposed by crosslinking.[57,111] Tu also utilized uncrosslinked linear polystyrene (LPS) seeds to create shape-changing JPs, highlighting the flexibility of uncrosslinked seeds in enabling phase separ-

ation and polymerization-induced morphology changes.[112] These studies collectively emphasize the benefits of using uncrosslinked seeds in Janus particle synthesis, offering tunable properties and diverse morphologies.

On the other hand, crosslinkers transform linear polymers into more rigid, temperature-resistant, and chemically stable particles, providing significant advantages in the synthesis of JPs. The degree of crosslinking in seed particles plays a crucial role in determining the final morphology of JPs. Higher crosslinking densities typically result in multilobe or raspberry-like structures, while lower densities favor dumbbell shapes. Additionally, crosslinked structures provide greater stability during polymerization, helping maintain well-defined Janus morphologies, especially in smaller particles.

Kim *et al.* explored the effect of seed crosslinking on monomer swelling and final particle morphology using a two-stage swelling method in seeded polymerization.[121] They found that varying the crosslinking density of seed particles, achieved by incorporating different concentrations of urethane acrylate (UA) as a crosslinker, significantly impacted monomer swelling behavior. Higher crosslinking densities led to reduced swelling capacity due to the increased elastic force of the polymer network, resulting in particles with less uniform and more complex morphologies, such as doublets or phase-separated domains. In contrast, lower crosslinking densities produced smoother, more spherical particles. Tu demonstrated that the crosslinking density plays a crucial role in the stability and functionality of the JPs' formation.[112] Similarly, Peng *et al.* utilized crosslinked poly(methyl methacrylate) (PMMA) spheres to produce complex shapes such as hamburger-like particles and clusters.[126] By controlling the degree of crosslinking, they could manipulate the formation of liquid protrusions, leading to the desired anisotropic structures.

These studies collectively show that the morphology of JPs is heavily influenced by the crosslinking density of the seed particles. The choice and concentration of crosslinkers directly impact swelling behavior and final morphology. Lower crosslinker ratios tend to favor spherical shapes due to more uniform swelling, while higher ratios result in less swelling and more rigid particles, often leading to raspberry-like structures with multiple smaller domains. This relationship allows for precise control over particle morphology in the synthesis of more complex JPs.

3.2. Second monomer

The selection of the second monomer is a crucial aspect of Janus particle synthesis, as it directly impacts not only the morphology but also the chemical functionality, surface properties, and overall application potential of the final particles. Different monomers introduce unique chemical groups to the particle surface, allowing for the customization of JPs to meet specific functional needs. For instance, incorporating hydrophobic monomers such as styrene or alkyl acrylates can create amphiphilic particles, which are particularly useful for stabilizing emulsions or forming self-assembled structures. Conversely, using hydrophilic monomers like acrylic acid or poly(ethylene glycol) can impart biocompatibility, making these particles suitable for biomedical applications such as drug delivery or biosensing.[127,128]

A wide range of monomers available for Janus particle synthesis are shown in Fig. 6, each contributing distinct functionalities that enhance the versatility of these particles. Monomers with reactive functional groups, such as epoxy or amine groups, allow for further chemical modifications post-synthesis, enabling the attachment of targeting ligands, fluorescent markers, or other functional molecules. Furthermore, by carefully selecting and combining different monomers, researchers can achieve precise control over phase separation and compartmentalization within the particles, which is essential for creating anisotropic structures with distinct physical

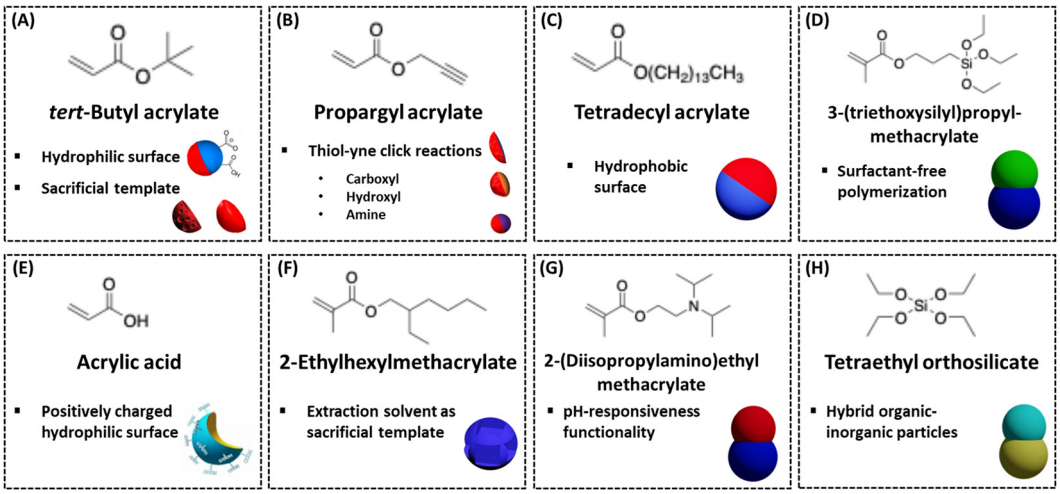

Fig. 6 Different choices of second monomers that can lead to JPs of different morphologies and functionalities in emulsion polymerization with different surfactant packages. (A) *tert*-Butyl acrylate,[112] (B) propargyl acrylate,[125] (C) tetradecyl acrylate,[57] (D) 3-(triethoxysilyl)propyl-methacrylate,[118] (E) acrylic acid,[113] (F) 2-ethylhexylmethacrylate,[129] (G) 2-(diisopropylamino)ethyl methacrylate,[130] (H) tetraethyl orthosilicate.[120]

and chemical properties. This control is critical for tailoring JPs to meet the demands of various applications, such as catalysis, where selective exposure of active sites is necessary, or environmental remediation, where particles may need to capture and remove contaminants from water. Thoughtful monomer selection and meticulous control over the synthesis process are key to realizing the full potential of JPs, enhancing their performance and efficiency in intended applications.

3.3. Solvent extraction

Particle morphology can be altered through solvent extraction techniques. For instance, Wang *et al.* developed a method for producing Janus-like polymer particles through internal phase separation and solvent extraction. The authors utilized an oil-in-water emulsion, where a polymer mixture, including PMMA and PS, was combined with hexadecane (HD) dissolved in dichloromethane (DCM). The evaporation of DCM induced phase separation within the emulsion droplets, leading to the formation of distinct polymer-rich regions. The innovative aspect of their approach involved extracting HD using hexane, which effectively removed the oil phase, resulting in the formation of JPs with controlled morphologies. They demonstrated that the morphology of these particles could be finely tuned by varying the emulsifier type and concentration, achieving structures such as hollow spheres, hemispheres, and truncated spheres.[131]

Following a similar strategy, 2-ethylhexylmethacrylate (EHMA) can be dissolved in organic solvents to create cavities or porous structures within JPs, enhancing their functionality for applications in drug delivery and catalysis. As shown in Fig. 7, Fujibayashi and Okubo investigated phase separation in seeded dispersion polymerization to control the shape of JPs.[129] By employing organic solvent droplets that are primarily absorbed by the second polymer phase, the study successfully produced non-spherical composite particles through solvent evaporation. The resulting particle shapes were influenced by factors such as the alkyl chain length, hydrocarbon type, and methanol/water ratio. This approach provided valuable insights into the thermodynamic and kinetic factors governing particle morphology, offering a versatile method for synthesizing complex particle shapes.

3.4. Sacrificial polymer templates

Sacrificial polymers can be used to create nonspherical JPs. These polymers are removed post-polymerization, leaving behind the desired polymer phase. As shown in Fig. 8, monomer *t*BA is widely used for generating sacrificial polymer templates. Upon acid hydrolysis, poly(*tert*-butyl acrylate) or P*t*BA converts to poly(acrylic acid) or PAA, which is highly water-soluble and can be easily removed. If a crosslinker is deployed in the synthesis, a robust network of covalent bonds is formed between polymer chains which hinders the dissolution of the PAA phase upon hydrolysis, so the PAA phase remains as a hydrophilic surface instead. Utilization of this feature with crosslinker allows for the creation of various structures and functionalities. Chen *et al.* utilized *t*BA in their synthesis protocols without any crosslinker and demonstrated the formation of uniform lens-shaped particles with tunable properties.[132] On the other side, Tu *et al.* showed that using crosslinker could help retain P*t*BA on the crosslinked PS seed surface as a hydrophilic counterpart.[112] Hamilton *et al.* also incorporated *t*BA as a second monomer in the seeded emulsion polymerization with non-crosslinked polystyrene (PS) seeds.[133] When only *t*BA was used in the monomer feed, it underwent homopolymerization, resulting in P*t*BA microdomains within the PS matrix, yielding patchy JPs. After acid-catalyzed hydrolysis, the removal of PAA created pores and cavities within the PS matrix, resulting in porous-bowl particles with a concavo-convex shape. The anisotropic colloids exhibit different internal structures depending on the monomer composition and concentration used. When styrene (Sty) was added to the monomer feed, the morphology transitioned from patchy-Janus to smoother spherical colloids, depending on the ratio of Sty to *t*BA.

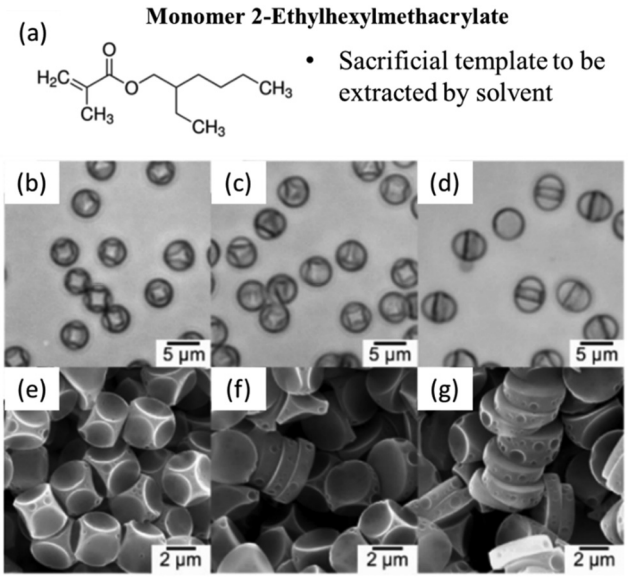

Fig. 7 Monomer selection of 2-ethylhexylmethacrylate (EHMA). (a). Molecular structure of the EHMA monomer. Optical micrographs (b–d) of PS/PEHMA/hexadecane composite particles and SEM photographs (e–g) of PS particles after the extraction of PEHMA and hexadecane with 1-butanol from PS/PEHMA composite particles prepared at various times of seeded dispersion polymerization in methanol/water (80/20, w/w) medium in the presence of hexadecane droplets: (b and e) 40 h, (c and f) 56 h, (d and g) 72 h. Reproduced from ref. 129 with permission from the American Chemical Society. Copyright 2007.

3.5. Kinetics control

Beyond thermodynamics, particle morphology is also shaped by the interplay of kinetic factors, such as the rate of monomer diffusion and polymerization. Li *et al.* studied the kinetics of JP formation using a seeded emulsion polymerization process.[124] Through combined experimental analysis and computer simulation, they discovered that the coalescence of small protrusions into a single large lobe is kinetically controlled by

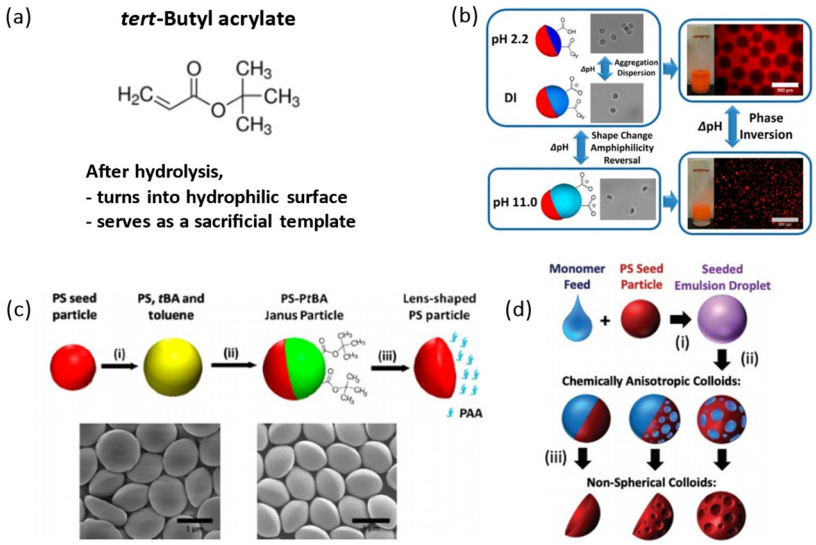

Fig. 8 Monomer selection of *tert*-butyl acrylate (*t*BA). (a) Molecular structure of *t*BA. (b) Shape-changing and amphiphilicity-reversing JPs with pH-responsive surfactant properties. Reproduced from ref. 112 with permission from the American Chemical Society. Copyright 2014. (c) Illustration of the synthesis of lens-shaped PS particles. Reproduced from ref. 132 with permission from the American Chemical Society. Copyright 2017. (d) Seeded emulsion polymerization and acid-etching of the polyacrylate phase. Reproduced from ref. 133 with permission from the Royal Society of Chemistry. Copyright 2019.

the diffusion rates of the polymer chains. The degree of crosslinking in both the seed and secondary polymers significantly impacts the final particle morphology. Highly crosslinked seeds tend to produce multilobe morphologies due to the reduced mobility of the protrusions. In contrast, lightly crosslinked seeds facilitate the formation of the thermodynamically favored dumbbell morphology, as the protrusions merge more easily. The formation of the final particle morphology is governed by the interplay between thermodynamic equilibrium and kinetic factors, including the mobility and diffusion of the polymer protrusions. The entanglement between the seed and secondary polymer networks significantly influences the viscoelastic properties of the protrusions, affecting their ability to merge. Ultimately, kinetic factors dictate the final morphology of JPs. By understanding and manipulating these factors, precise control over particle morphology can be achieved as illustrated in Fig. 9.

3.6. Mathematical models and computer simulations

The intricate interplay between kinetics, thermodynamics, and molecular transport in multistage emulsion polymerization poses significant challenges to experimental investigation. In contrast, computer simulation can isolate and elucidate competing effects, making them indispensable for establishing a clear reaction–morphology relationship. Various models have been developed to predict particle morphologies based on thermodynamic equilibrium conditions, assuming that phase-separation kinetics is much faster than polymerization kinetics. These models, while effective in predicting equilibrium morphologies and conversion-dependent structures, lack dynamic information and cannot capture the formation of morphology in real time. Moreover, they fall short of predicting nonequilibrium, kinetic-controlled morphologies, as they assume that equilibrium is reached instantaneously, without restrictions on polymer chain diffusion or cluster migration.

To address these limitations, new models have been developed that incorporate kinetic factors, such as the location of polymer formation and the rates of both polymer diffusion and cluster migration, to better predict particle morphology. González-Ortiz and Asua introduced a series of increasingly complex models to account for cluster migration, polymerization reactions, cluster nucleation, and chain diffusion.[134–136] Their initial model described the migration of polymer clusters in a nonreacting composite particle dispersed in an aqueous phase, governed by the balance between van der Waals forces and viscous forces. This model tracked cluster motion *via* an overdamped Langevin equation, considering interactions with other clusters and the aqueous phase. Their simulations demonstrated that the dynamics of cluster migration heavily depends on the viscosity of the polymer matrix.[134]

The model was later extended to a reactive system, incorporating the effects of polymerization concurrent with cluster migration. Here, a seed of polymer 2 was swollen by monomer 1, which was converted into polymer 1. The model, which neglected cluster nucleation, assumed preformed, equal-sized clusters of polymer 1 within each particle. As polymerization proceeded, polymer 1 was produced in both clusters and the polymer 2 matrix. This version of the model combined the balance of forces governing cluster motion and coagulation with material balances describing polymerization, considering monomer swelling effects on interfacial tensions and vis-

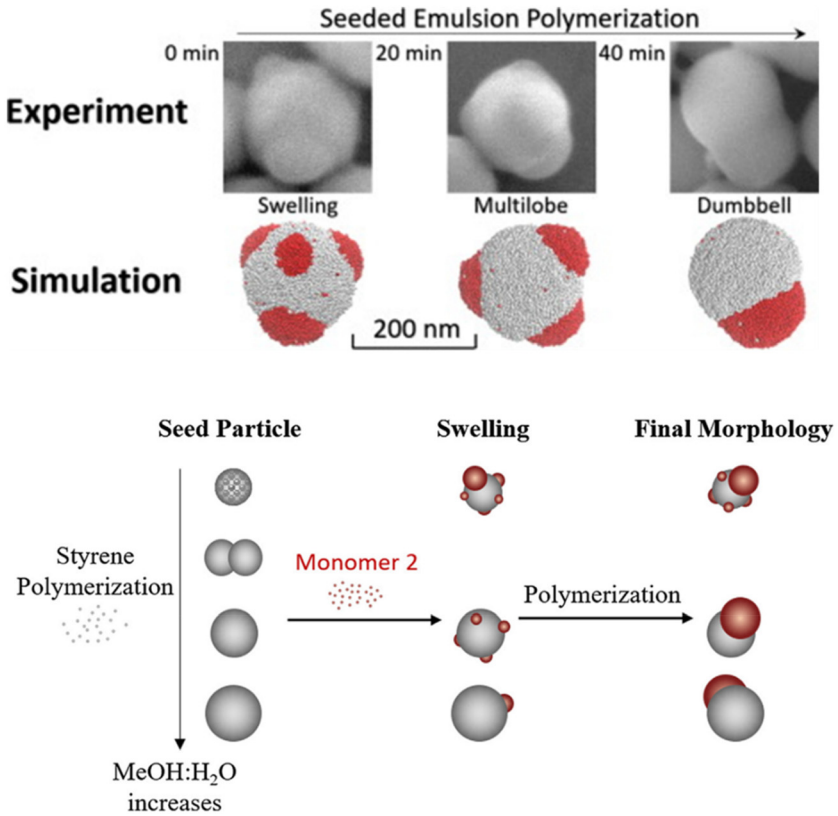

Fig. 9 Schematic illustration of morphology evolution during the seeded emulsion polymerization. The morphologies are significantly impacted by the crosslinking density and solvent choice during seed synthesis. The morphology can be controlled through polymerization kinetics. Reproduced from ref. 124 with permission from Elsevier. Copyright 2019.

cosity.[136] The model was further refined to include cluster nucleation and finite rates of polymer diffusion, applied to simulate batch emulsion polymerizations of methyl methacrylate on a polystyrene seed. The results showed that final particle morphology is highly dependent on kinetic factors: slower polymerization rates led to morphologies closer to equilibrium, while initial cluster volume and nucleation rates had less impact.

Sundberg's group incorporated the concept of limited radical penetration to model morphology development in phase-separated latex particles under kinetically controlled conditions.[137] Very slow diffusion rates for the radicals within the particles after entering from the water phase and surface anchoring of the radicals due to the presence of charged end groups on the chains could prevent radical penetration into the seed particles, resulting in a spatial gradient in radical concentration. They developed a set of differential equations to model the kinetics of seeded emulsion polymerization, considering reactions in both aqueous and polymer phases. This approach allowed them to predict radial density distributions of termination events, which influenced the final particle morphology. Although their model successfully predicted polymerization kinetics and morphology development, it did not account for the coalescence of phase-separated domains due to polymer diffusion and thermodynamic rearrangement. To address these gaps, a Monte Carlo approach was later implemented to replace the differential equations, enabling the modeling of simultaneous reaction steps and diffusion events that control morphology development, including complex chain transfer reactions.[138]

Previous models were only able to predict the detailed morphology evolution of a single particle, which provides limited insights into a real system that contains a distribution of particle morphologies. To overcome this limitation, Hamzehlou *et al.* developed a new model to account for diverse morphologies of the whole population of polymer particles.[139] The key idea of their model is to describe the distribution of particle morphologies by a distribution of phase-separated clusters of newly formed polymer dispersed in the seed particle. According to their position in the particles, the clusters are divided into two different categories: those that are at equilibrium positions and clusters at nonequilibrium positions. The equilibrium position is determined by thermodynamics. The number and weight distributions of the equilibrium and nonequilibrium clusters are separately calculated by considering all relevant kinetic events, including cluster nucleation, polymerization, polymer diffusion, and cluster coalescence. This model was applied to polymer–polymer latex particles obtained in both seeded emulsion polymerization and miniemulsion polymerization.

In contrast to the continuum modeling described above, microscopic particle-based simulations were also developed to model morphology development. Duda and Vázquez introduced a two-dimensional off-lattice Monte Carlo (MC) model of equilibrium morphology by representing the mixture of latex constituents and water as nonadditive hard-sphere fluids.[140] The polymers of different species were modeled as chains of freely-jointed beads, while water was modeled by an ensemble of individual beads. The flexibility of polymer chains can be tuned by varying the distance between two adjacent beads. The relative hydrophilicity of chains was readily controlled by the nonadditive parameters. A special Metropolis MC step was designed to provide adequate sampling of the phase space for long chains and high density states. Herrera *et al.* and Reyes and Asua further extended this model to three-dimensional systems with three or more phases, such as polymer–polymer and polymer–polymer–inorganic hybrid multiphase particles.[141,142] It was shown that this simple model was capable of reproducing the key features of the equilibrium morphologies observed in experiments.

Although efficiently predicting the equilibrium morphology of composite polymer particles, the MC method cannot resolve the dynamics of the system. Akhmatskaya and Asua simulated the dynamic evolution of the particle morphology of multiphase polymer–polymer and polymer–inorganic systems using stochastic dynamics in which the movement of phases was described by the Langevin equation.[143,144] The simulation adopted a highly coarse-grained representation of the initial state, a polymer seed particle (polymer 1) swollen with a second monomer (monomer 2) or a mixture of monomer and other inorganic materials. The system consists of spherical subparticles of the same size interacting with its neighbors. Each subparticle of different types represents either a group of monomer molecules, a cluster of water molecules, or an individual polymer chain. This mesoscopic model bridges the disparate length scales between polymer chains and the whole particle. Polymerization of monomer 2 was simulated by converting the monomer subparticles into subparticles of a new polymeric phase (polymer 2). Namely, a new type of subparticle appeared in the system as a result of the reaction, but the total number of simulated subparticles was constant during the simulation process. Polymerization kinetics was accounted for by means of the rate of transformation of monomer 2 subparticles into subparticles of polymer 2. The effect of the internal viscosity of the particle on the mobility of phases was modeled using an empirical equation that relates viscosity increase to the conversion of monomer.

Li *et al.* combined the single-bead (*i.e.*, one-subparticle) polymer chain model with reactive dissipative particle dynamics (DPD) to simulate the phase separation of PS and P*t*BA in seeded emulsion polymerization and the formation of multilobed JPs under nonequilibrium conditions.[124] Soft-core pairwise interactions between DPD beads (subparticles) provided a quantitative means to control the Gibbs free energies of mixing between the seed polymer, second monomer, and second polymer, as well as the interfacial tensions between different phases. Similar to Akhmatskaya and Asua, polymerization was simulated by the simple conversion of bead types from monomer to polymer. To account for the effect of crosslinking in both seed particle and second-stage polymerization, the formation of the polymer network was modeled by forming permanent bonds between polymer beads and crosslinkers. Induced by polymerization, the seed polymers and the second polymers underwent phase separation, which resulted in particle morphology evolution. A dynamic bond model was introduced to capture entanglements between the seed and second polymer networks, which significantly influenced the viscoelasticity and dynamics of phase-separated clusters (Fig. 10). The simulation demonstrated that the multilobe morphology was in a state of nonequilibrium and kinetically controlled by diffusion of the second polymer protrusions on the seed particles. A more recent study by Nedyalkova *et al.* investigated the effect of surfactants on the morphological evolution of the polystyrene–poly(methyl methacrylate) particle shape at the molecular level using full-atom molecular dynamics.[145] The simulations were carried out in three stages to assess the role played separately by the PS core and the surfactant used during the process followed by the addition of the MMA to the PS core/surfactant system and finally by the substitution of MMA with PMMA in the system. The results revealed the growth of a single PMMA patch and the presence of surfactants as key elements in forming a Janus particle.

4. Functionalization and applications

Functionalization of JPs can be achieved either through the use of functional monomers or by post-synthesis surface modification. Introducing functional groups *via* monomers presents a challenge, as these groups can influence phase separation and may not always result in a well-defined Janus morphology. Consequently, post-surface modification offers a more versatile

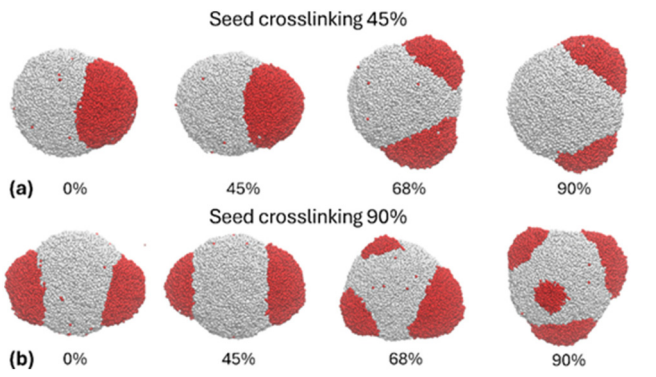

Fig. 10 The DPD simulations showing the effect of polymer chain entanglements between the seed (white beads) and second polymer (red beads) networks on the distinct final morphologies of JPs for crosslinking degrees of 0%, 45%, 68%, and 90% for the second polymer. Panels (a) and (b) compare the 45% and 90% crosslinked seeds, respectively. Reproduced from ref. 124 with permission from Elsevier. Copyright 2019.

and reliable approach for achieving the desired functionalization.

4.1. Post-functionalization

Modifications of JPs enable a high degree of customization, which is crucial for applications such as drug delivery, where particles must interact with specific biological targets, or catalysis, where functional groups act as active sites for chemical reactions. For example, Jiang *et al.* utilized surface modification techniques on PS seeds to create JPs with tailored surface properties, enhancing their utility in drug delivery and biosensing.[114] Wu *et al.* employed modified seed particles to develop JPs with pH-triggered switchable amphiphilicity for interfacial applications.[130,146] They synthesized polystyrene-poly(2-(diisopropylamino)ethyl methacrylate)/poly(3-(triethoxysilyl)propyl methacrylate) (PS-PDIPAEMA/P(3-TSPM)) JPs using surfactant-free emulsion polymerization and phase separation. The modified seeds, composed of PS-PDIPAEMA, were designed to respond to pH changes, allowing the nanoparticles to switch their amphiphilicity on or off. At low pH values, the nanoparticles became more hydrophilic, enhancing their interfacial activity, while at higher pH values, they became more hydrophobic.

As shown in Fig. 11, Honciuc *et al.* explored the selective modification of JPs with polyaniline (PANI) to create conductive and non-conductive lobes.[118,147] This selective functionalization enabled the creation of microcapsules *via* Pickering emulsion polymerization, showcasing the potential for designing multifunctional particles with distinct properties on each lobe.

As shown in Fig. 12, post-modification of JPs can be achieved through techniques such as nanoparticle grafting, hydrolysis, and *in situ* surface polymerization, each offering distinct advantages. Nanoparticle grafting enhances functionality for applications like drug delivery and catalysis, while acid hydrolysis allows for the selective conversion of specific domains, providing pH-responsive behavior and tunable surface functionalities. *In situ* surface polymerization enables

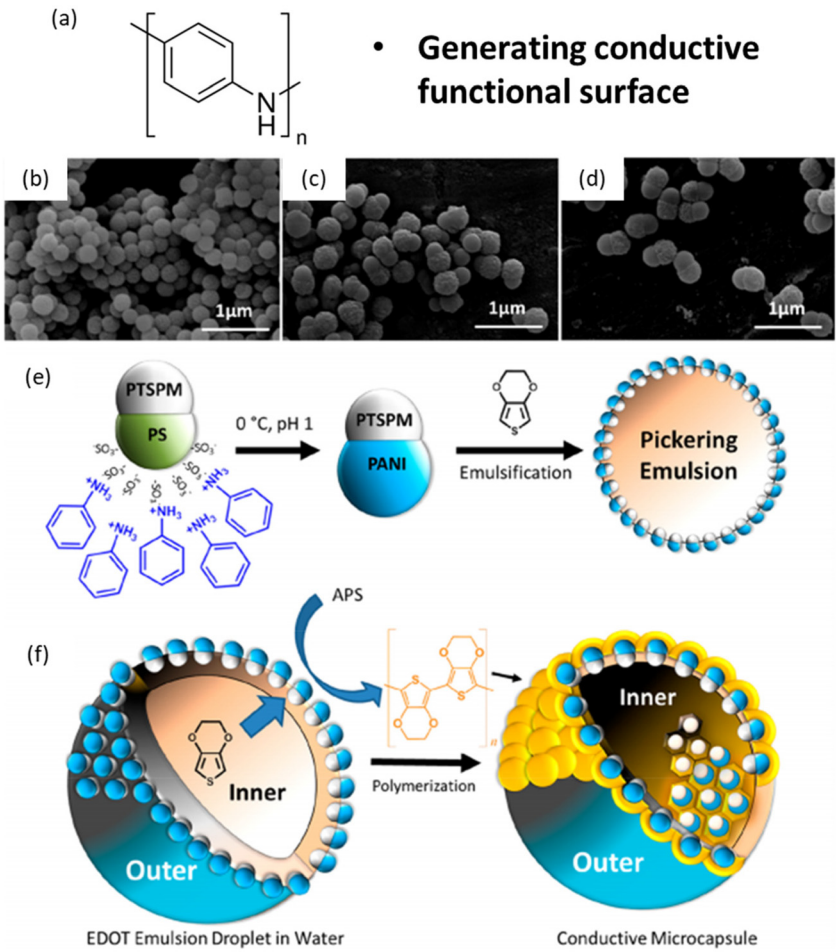

Fig. 11 Seed modification-PANI. Structure of nanoparticles and formation of microcapsules. (a) Molecular structure of EHMA monomer. SEM images of (b) seeds, (c) JPs-1, (d) JPs-2. (e) Reaction scheme for the selective modification of JPs with PANI. The PANI JPs are next used for the emulsification of EDOT. (f) Interfacial polymerization and formation of microcapsules with a honeycomb structure of the inner wall. In panels b and c, the PTSPM Janus lobe appears to be brighter than the PS Janus lobe due to a higher electron density. Reproduced from ref. 147 with permission from the American Chemical Society. Copyright 2019.

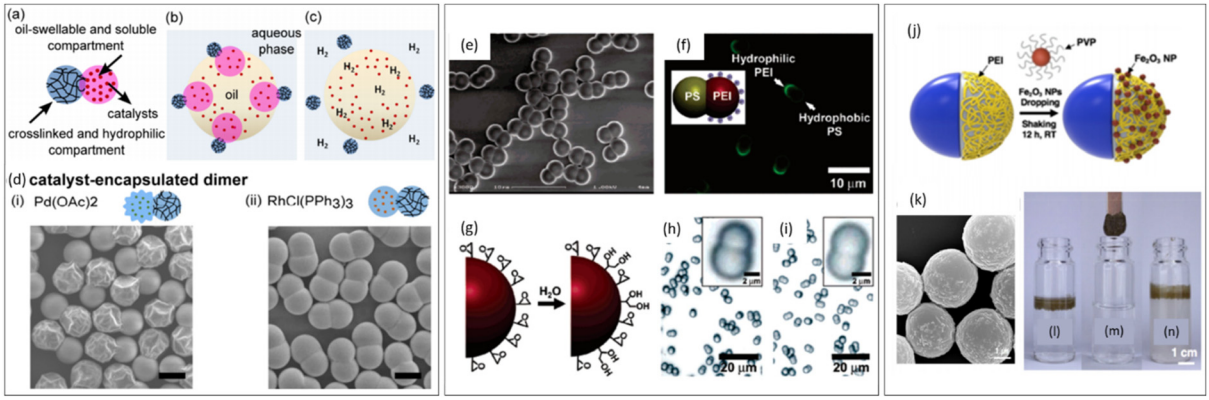

Fig. 12 Post-treatment of JPs by surface grafting. (a–c) Schematic illustration of bicompartmental vehicles for the delivery of catalysts to the oil phase and photographs of oil-phase delivery of the Wilkinson's catalyst and hydrogenation reaction. (d) Encapsulation of two molecular catalysts in the un-cross-linked lobe. Scale bar for all images: 2 μm. Reproduced from ref. 47 with permission from the American Chemical Society. Copyright 2019. (e–h) Amphiphilic PS dumbbell particles obtained by the reaction of the epoxy groups with PEI. Reproduced from ref. 123 with permission from the American Chemical Society. Copyright 2006. (i–n) Grafting magnetic iron oxide particles for patchy Janus colloid surfactants for the reversible recovery of Pickering emulsions. Reproduced from ref. 111 with permission from the American Chemical Society. Copyright 2018.

the creation of conductive and optoelectronic layers, broadening the applications of JPs in electronic and sensor technologies.[47,111,123]

As shown in Fig. 13, Bradley *et al.* demonstrated the use of propargyl acrylate in the synthesis of clickable JPs, which were subsequently functionalized with thiols using thiol–yne click reactions.[125] This modification introduced carboxyl, hydroxyl, or amine groups to the particles, significantly enhancing their amphiphilicity. The resulting particles were particularly effective in stabilizing emulsions by maintaining stable interfaces between polar and non-polar phases. This approach underscores the efficiency of click chemistry in producing functionalized JPs with diverse applications.

Hamilton *et al.* employed acid-catalyzed hydrolysis (ACH) to modify JPs and reveal their internal morphology.[133] This post-synthetic modification exposed microdomains within the col-

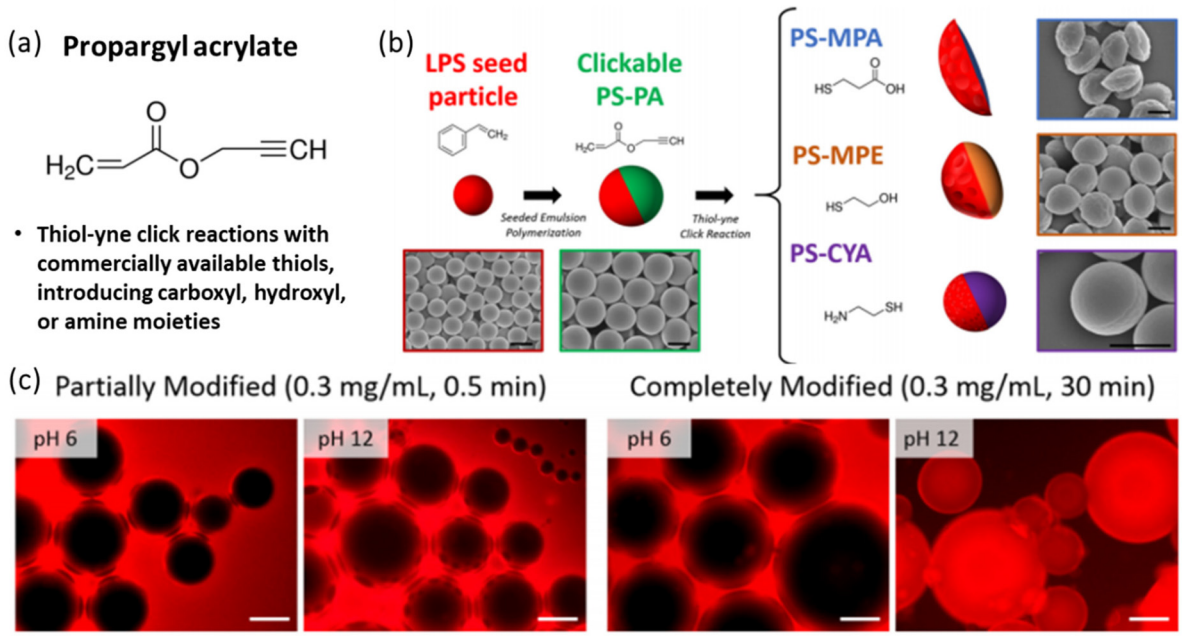

Fig. 13 Monomer selection of propargyl acrylate (PA). (a) Molecular structure of PA. (b) Schematic and corresponding SEM images depicting the synthesis of clickable PS–PA JPs and subsequent modification *via* thiol–yne click reactions. The LPS particles are spherical, while all the JPs are non-spherical. Scale bars on the SEM images represent 1 μm. (c). Fluorescence microscopy images of water and toluene emulsions stabilized by PS-MPA particles. The dark regions represent the water phase, and the bright regions represent the toluene phase containing 1 wt% Nile Red. Scale bars represent 100 μm. Reproduced from ref. 125 with permission from the American Chemical Society. Copyright 2019.

loids, allowing for a detailed examination of the phase-separated structures. The study demonstrated that varying the monomer feed composition influenced the phase separation dynamics and ultimately the particle morphology.

4.2. Interfacial catalysis

Owing to the excellent catalytic properties of metallic components (*e.g.*, Pt, Pd and Au) for reactions such as organic synthesis and hydrogenation, inorganic JPs have shown great promise in interfacial catalysis. Janus-type catalysts present unique advantages in catalytic applications due to their asymmetric structure, which provides distinct functional domains within a single particle. These catalysts enhance the accessibility of reactants to active sites, improve phase selectivity, and offer high interfacial activity, making them particularly effective for interfacial catalysis. Their ability to stabilize emulsions and the ease of recovery and reuse further enhance their practical applicability.[90,148,149]

The amphiphilic JPs, which exhibit the surfactant-like property for the stabilization of the biphasic emulsion reaction system, can increase the reactive interface area and kinetics. As a result, amphiphilic JPs often result in a drastic improvement in catalytic efficiency when compared with homogenous nanoparticles that are unable to stabilize the emulsion. Moreover, other properties of JPs, such as magnetic and plasmonic characteristics, provide additional functionalities to manipulate interfacial catalysis in emulsions. Compared with traditional molecular surfactants, one of the biggest advantages of JPs is their considerably larger sizes, making it easier to separate and recycle the catalysts from solution *via* filtration. It is even more efficient to collect the catalysts by an external magnetic field when they are magnetic responsive. Zhao *et al.* synthesized dual-mesoporous Fe_3O_4@mC&mSiO_2 JPs as "magnetic solid surfactants," which are made up of a mesoporous SiO_2 nanorod and a core–shell structured Fe_3O_4@mC nanosphere.[150] Further loading of Pt nanocrystals into the hydrophobic carbon domain enabled the catalytic reduction of 4-nitroanisole to 4-nitroanisole with $NaBH_4$ at the oil–water interface, giving a 100% conversion efficiency. In contrast, the conversion efficiency dropped to less than 10% when non-amphiphilic catalysts (*e.g.*, Pt-loaded Fe_3O_4@mC core–shell nanoparticles) were used, indicating the great advantage of amphiphilicity for the biphasic emulsion reaction system. The JPs could be easily collected by an external magnetic force for reuse and showed almost constant catalyst efficiency during the tested 10 cycles. When another active catalytic site was introduced by forming $-NH_2$ active groups in the hydrophilic mesoporous mSiO_2 domain, a unique design of solid surfactants with dual catalytic properties was achieved. This enabled biphasic cascade reactions catalyzed by solid surfactants at the oil–water interface, which avoided complicated and repeated purification processes to transfer intermediates between different reaction systems. Notably, the fabricated JPs showed outstanding performances in the biphasic cascade synthesis of cinnamic acid with a high turnover frequency of 700 h^{-1}. More interestingly, the dual-mesoporous Fe_3O_4@mC&mSiO_2 JPs may be used as a universal platform for various biphasic cascade reactions, as the desired catalysts can be easily loaded into the hydrophobic and hydrophilic domains in the JPs.

Additionally, when photocatalytic metal oxides (*e.g.*, TiO_2 and ZnO) are incorporated into JPs, catalytic degradation of dyes at emulsion interfaces can be realized. Zhou *et al.* reported the synthesis of methyl-capped Janus TiO_2–SiO_2 particles and used them as emulsifiers and photocatalysts simultaneously.[151] The SiO_2 side was found mostly facing toward the oil phase, while the TiO_2 part faced toward the water phase. Such a preference in the orientation of Janus TiO_2–SiO_2 particles at the oil–water interface facilitates the photocatalytic reaction in the aqueous phase, as the photocatalytic TiO_2 part stays away from the oil phase and interacts more with water. Under UV radiation, the photocatalysis process in the stirred aqueous system only takes 50 min to thoroughly degrade water-soluble methyl blue, faster than that in the static emulsion system (180 min).

In the study by Liu *et al.*, two types of Janus-type catalyst were synthesized using snowman-like SiO_2@PDVB/PS JPs as the support.[14] The functionalization process involved selectively modifying the silica hemisphere with amino groups to facilitate the *in situ* growth of gold nanoparticles (Au NPs). The catalytic performance of these Janus-type catalysts was evaluated in both homogeneous and interfacial reaction systems using the reduction of nitro-compounds as model reactions. The results demonstrated that the Janus-type catalysts exhibited excellent catalytic activity in homogeneous systems and were easily recyclable. Moreover, the catalysts showed significantly higher catalytic efficiency at the emulsion interface compared with the oil–water biphasic interface, attributed to the enhanced accessibility of reactants to the exposed Au NPs on the JPs (Fig. 14). Wu *et al.* presented an efficient method for fabricating JPs with active groups using an oil-in-water emulsion system.[152] By employing glycidyl methacrylate (GMA) and (perfluorodecyl) ethyl acrylate (FC) as monomers, JPs were synthesized through UV-induced free radical polymerization in the presence of a composite surfactant solution comprising sodium dodecyl sulfate (SDS) and Zonyl FS-300. This approach facilitated precise control over droplet morphology by adjusting the surfactant-to-monomer ratio, resulting in various emulsion types including Janus emulsions. The presence of epoxy groups on the particles allowed for selective post-functionalization, producing amphiphilic PFC-PGMA-JPs. These particles demonstrated exceptional capabilities in stabilizing emulsions and significantly enhanced catalytic efficiency when loaded with gold nanoparticles (PFC-PGMA-NH_2@Au), achieving a conversion rate of 84.13% for the reduction of 4-nitrophenol. Kirillova *et al.* reported on the design of hybrid JPs decorated with metallic nanoparticles for catalytic applications.[21] The Janus particles consisted of a silica core with two distinct polymeric shells: hydrophilic poly(acrylic acid) and hydrophobic polystyrene. Silver (Ag) or gold (Au) nanoparticles were selectively immobilized into the hydrophilic polymer shell, creating a stimulus-responsive catalytic system.

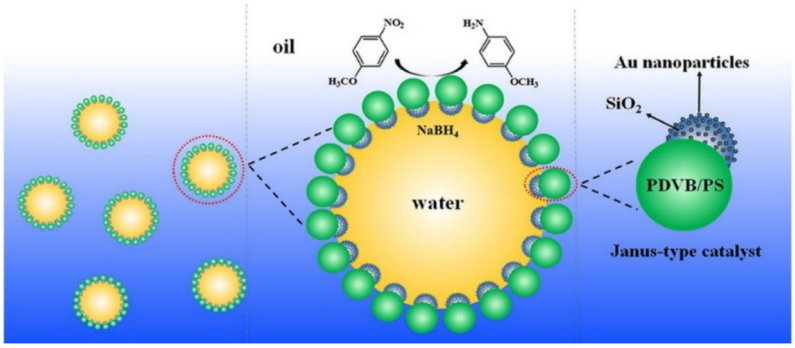

Fig. 14 Schematic illustration of how the Janus-type catalyst can stabilize a water-in-oil emulsion and exhibit high catalytic activity for the reduction of nitro-compounds at the emulsion interface. Reproduced from ref. 14 with permission from Elsevier. Copyright 2017.

4.3. Emulsion stabilizers

JPs have long been employed as stabilizers in emulsions, where they demonstrated exceptional performance. Early calculations have shown that JPs with the optimized Janus balance can have 3 times higher adsorption energy at the interface than their homogeneous counterpart.[5] Taking advantage of such a significant adsorption energy at the oil/water interface, the JPs effectively suppressed aggregation and coalescence, leading to well-defined latex particles with high monodispersity and long-term stability. Walther *et al.* developed JPs that showed excellent stabilization for emulsion polymerizations.[153] Lan *et al.* investigated the emulsification properties of amphiphilic JPs synthesized *via* seeded emulsion polymerization.[66] The JPs, composed of hydrophilic poly(acrylic acid) and hydrophobic polystyrene domains, were designed to study the effect of their configuration on emulsion stabilization. It was found that JPs with a higher Janus balance (larger hydrophilic domains) stabilized oil-in-water emulsions, while those with a lower Janus balance (larger hydrophobic domains) stabilized water-in-oil emulsions. Lotierzo *et al.* synthesized Janus and patchy particles using nanogels as stabilizers in emulsion polymerization.[154] The nanogels were made by the covalent cross-linking of block copolymer micelles. These nanogels, with distinct functional patches, served as stabilizers during the emulsion polymerization of styrene, resulting in anisotropic Janus and patchy colloids.

The ability to tune the hydrophilic and hydrophobic domains of JPs allows for precise control over emulsion types, enhancing their versatility for various industrial applications. Their exceptional performance in stabilizing emulsions underscores their potential for use in pharmaceuticals, food processing, cosmetics, and other fields where stable emulsions are crucial.

4.4. Diagnosis and therapy

Inorganic JPs that incorporate multiple functional components have been widely studied in diagnosis and therapy, including biosensing, bioimaging, drug delivery, cancer therapy, and combined theranostics. A fascinating advantage of JPs is that they combine multiple functionalities within one nanoparticle platform, thus enabling more rapid, precise, and efficient diagnosis and therapy. While numerous studies on inorganic JPs in the past two decades have demonstrated their extraordinary capabilities and great potential, those JPs are usually considered to be chemically homogenous (*i.e.* hydrophilic) on their surfaces. Recently, there is a growing interest in taking advantage of the amphiphilicity of JPs, as they may behave drastically differently when interacting with cell membranes and offer unique benefits. It was demonstrated that amphiphilic JPs with the spatial segregation of surface chemistry caused nanoparticles to bind more strongly to lipid membranes and induce defects more effectively than their surface homogenous counterparts.[155] The increase in Janus balance, *i.e.* more hydrophobicity in the nanoparticles, induced more defects at lower threshold concentrations.[156] These studies indicate that amphiphilic JPs can significantly influence the cellular uptake mechanism and uptake pathways. Another big advantage of amphiphilic JPs is that loading both hydrophobic and hydrophilic drugs becomes much easier because of their dual surface properties, thus realizing the optimal sequential therapy.[157] Similar to their molecular counterparts such as lipids, amphiphilic JPs tend to self-assemble into micelle-like nanostructures, which can be used for encapsulating drugs for controlled delivery. More intriguingly, amphiphilic JPs are stimulus-responsive due to their inorganic components, making it possible to trigger the drug release on demand by external environments. Self-assembly can also improve the communication of the component when it stays close, potentially enhancing the properties. In a typical platform of amphiphilic Janus Au–Fe_3O_4 nanoparticles which are modified with bicompartmental polymer brushes to produce opposite surface properties on the Au and Fe_3O_4 surfaces, Song *et al.* demonstrated the fabrication of two kinds of double-layered plasmonic-magnetic vesicle with Au or Fe_3O_4 localized dominantly on the outer or interior surface of the vesicular shell.[158] The vesicles exhibited enhanced physical properties (SERS, optical, photoacoustic and magnetic activities) compared with discrete Au–Fe_3O_4 nanoparticles, which can be attributed to the strong interparticle plasmonic coupling of the Au domains

and magnetic dipole interaction of the Fe_3O_4 domains. It is also possible to reverse the formation of vesicles by disassembling the JPs *via* external stimuli, as demonstrated by the platforms of pH-responsive Janus Au–Fe_3O_4 nanoparticles and ultrasound/glutathione dual-responsive Janus Au–MnO nanoparticles.[159] Such a disassembly process enabled the controlled release of drugs, which were pre-encapsulated into the vesicles. The simultaneous release of other species, such as smaller Au nanoparticles, Fe^{2+}, and Mn^{2+}, further improved the therapeutic efficacy *via* synergistic sonodynamic/chemodynamic therapies.[160]

Zhang *et al.* synthesized uniform Au@poly(acrylic acid) (PAA) JPs using a facile and scalable method.[161] These JPs were employed as templates to preferentially grow a mesoporous silica ($mSiO_2$) shell on one side and Au branches on the other, achieving distinct compartmentalization. The mesoporous silica was selectively modified with methoxy-poly(ethylene glycol)-thiol (PEG) and lactobionic acid (LA), enhancing stability, biocompatibility, and targeted delivery. The resulting multifunctional PEG-Au-PAA/$mSiO_2$-LA JP demonstrated pH and NIR dual-responsive drug-release properties, making them efficient for chemo-photothermal cancer therapy both *in vitro* and *in vivo*.

Hu and Gao reported the synthesis of compact nanocomposites with spatially separated functionalities for combined imaging and magnetolytic therapy.[162] They utilized a microemulsion technique, incorporating magnetic nanoparticles (MNPs) and fluorophores into distinct compartments. This approach maintained the individual optical and magnetic properties of the components. The resulting JPs exhibited a uniform size and demonstrated effective magnetic field modulated imaging and innovative cancer cell therapeutics, leveraging magnetically controlled mechanical forces for therapy. JPs offer significant potential in diagnosis and therapy applications due to their anisotropic surface properties and multifunctionality. The ability to combine distinct materials and functionalities within a single particle enables targeted delivery, imaging, and combined therapeutic approaches (Fig. 15).

4.5. Surface coating

Kirillova *et al.* developed hybrid hairy JPs specifically designed for anti-icing and de-icing surface coatings.[163] These particles featured a solid SiO_2 core with hydrophilic and hydrophobic polymer shells grafted onto opposite sides. The synthesis process involved creating the SiO_2 core using the Stöber method, followed by a Pickering emulsion approach and polymer grafting *via* ATRP. This method produced JPs with distinct amphiphilic properties, which, when applied to coatings, formed heterogeneous surfaces. These surfaces effectively reduced ice adhesion by promoting controlled ice nucleation and growth, making the coatings highly resistant to ice formation and easy to de-ice. The hydrophilic polymer shell collected water droplets, allowing them to spread and form large ice crystals that could be easily removed, offering an efficient solution for passive anti-icing applications.

In a different approach, Berger *et al.* engineered ultrahydrophobic functional coatings by controlling the aggregation of bicomponent core/shell JPs.[164] These particles were synthesized with PS and poly(2-vinylpyridine) (P2VP) shells using a grafting-from approach to ensure high grafting density

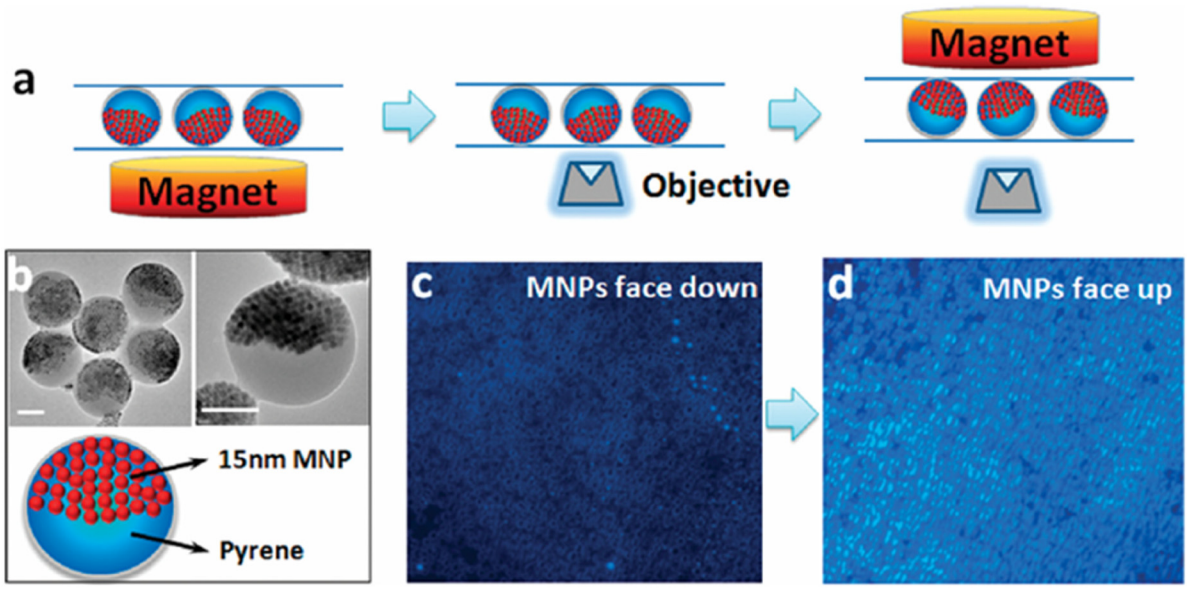

Fig. 15 Orientation-dependent fluorescence of magneto-optical biphasic nanocomposites. (a) Schematic of nanocomposite orientation modulation with magnetic fields. The magnetic segment blocks both excitation and fluorescence when it is facing down but has no effect on fluorescence when facing up (not in the light path). (b) TEM images of the nanocomposites with the two phases of similar volume. Scale bar 100 nm. (c) and (d) Fluorescence imaging of nanocomposites of opposite orientations. Reproduced from ref. 162 with permission from the American Chemical Society. Copyright 2010.

and stability. The particles were dispersed in a solvent compatible with the hydrophilic polymer shell to maintain colloidal stability and prevent premature sedimentation. Upon deposition on silica wafers pre-coated with thin polymer layers, the JPs self-assembled into hierarchically structured aggregates. This controlled aggregation led to the formation of rough layers with fractal characteristics, imparting ultra-hydrophobic properties to the coatings. The study showed that the wettability and surface morphology of the coatings could be finely tuned by adjusting the chemical structure of the polymers grafted onto the JPs, the nature of the substrate, and the degree of aggregation. Zhao *et al.* created cone-like Janus composite particles through an emulsion polymerization-induced phase separation technique, aimed at fabricating robust surface coatings with tunable wettability.[165] The process began with the synthesis of PS particles in the dispersed paraffin phase, which migrated towards the emulsion interface due to the Pickering effect. At the triple-phase contact line, an interfacial tension mismatch caused the particles to deform into a cone shape, with the hydrophilic side protruding and the hydrophobic side adhered to the paraffin surface. This unique shape allowed for selective modifications on the cone surface while protecting the flat side, resulting JPs with distinct hydrophilic and hydrophobic regions. These particles self-organized into superstructures in dispersions and were used to create coatings by spraying them onto a substrate pre-coated with epoxy resin. JPs covalently bonded to the substrate, forming a durable coating with adjustable wettability, ranging from highly adhesive to superhydrophobic, simply by altering the particle size distribution.

Yang *et al.* demonstrated a one-step approach for the large-scale fabrication of robust superhydrophobic coatings using strawberry-like JPs.[166] These particles were synthesized *via* a self-organized sol–gel process at a patchy emulsion interface, creating hemispherical particles with a coarse hydrophobic side and a flat hydrophilic side. The hydrophilic side was modified with imidazoline groups to enable covalent binding to substrates through cationic crosslinking with epoxy resins. Upon deposition on substrates coated with a thin layer of epoxy resin, the JPs self-organized into a monolayer, with the hydrophobic side facing outward. This configuration resulted in coatings that exhibited remarkable superhydrophobic properties, effectively mimicking the lotus leaf's ability to repel water.

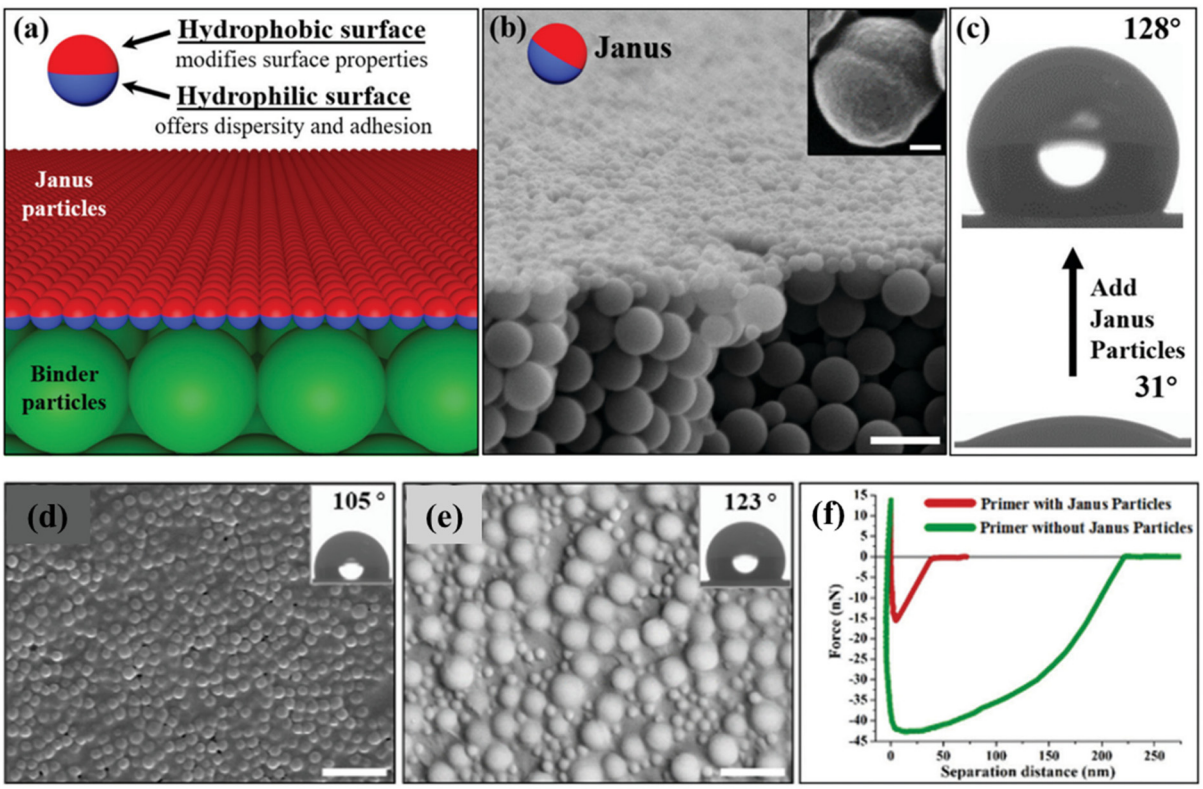

Fig. 16 (a) Schematic diagram for the coating structures formed by the self-stratification of amphiphilic JPs mixed with binder particles. (b) SEM image of the cross-section view of the dried coating structures. Scale bar is 2 mm. Inset shows the asymmetric morphology of a typical Janus particle with Janus balance (percentage of hydrophobic surface area) ~50%. Scale bar is 100 nm. (c) Contact angles of the coating surface before and after adding the JPs. (d and e) SEM images of coating films formed by commercial primer binder with added JPs, and force profiles measured on film surfaces using AFM: (d) commercial primer with 400 JPs added; (e) commercial primer with both 400 nm and 1.0 JPs added; scale bars are all 2 mm. (f) Representative force–distance curves recorded during retraction of an AFM tip from the coating film surfaces. Reproduced from ref. 122 with permission from the Royal Society of Chemistry. Copyright 2020.

4.6. Stratification and surface functionalization

Although previous uses of JPs as coating materials have shown promising results, their application has been limited by the complexity of surface treatments, which hinders large-scale industrial adoption. The properties of the final coating films are highly sensitive to experimental conditions, making broad and practical implementation challenging. Additionally, covering large surface areas requires significant quantities of JPs, making the process costly.

Recent work by Li *et al.* explored the self-stratification of amphiphilic JPs to create robust hydrophobic coatings.[122] Instead of using JPs as the sole coating material, they were employed as additives in conventional binder polymers. During the drying phase, a unique stratification process was observed, where most of the JPs quickly migrated to the air–water interface, orienting their hydrophobic sides outward to form a densely packed monolayer. This stratification significantly increased the water contact angle, enhancing the hydrophobicity of the coating surface. Importantly, because the majority of JPs are concentrated at the interface, they do not affect the bulk properties of the coating. By carefully designing the hydrophilic side for optimal adhesion, more robust water-resistant coatings can be achieved. The study demonstrated that these coatings retained their high contact angle and structural integrity even after solvent rinsing, highlighting the durability of the self-stratified Janus particle layer. This innovative method offers a cost-effective and commercially scalable solution for creating advanced hydrophobic coatings with strong adhesion and improved surface properties, suitable for a wide range of industrial and consumer products (Fig. 16).

5. Perspectives

This review highlights key advancements in Janus particle (JP) synthesis, particularly through methods like seeded emulsion polymerization, which enable the production of particles with diverse morphologies and tailored functionalities. JPs have already shown clear advantages over conventional particles in areas such as emulsion stabilization, catalysis, and drug delivery. Emerging fields such as additive manufacturing and battery technology are yet to be explored for their potential application. Despite the progress in JP synthesis and application, several critical gaps persist. One of the primary challenges is scaling up JP production while maintaining consistent, high-quality morphology and properties, as most current methods are still confined to small lab-scale tests. Furthermore, the long-term stability of JPs across various application conditions remains to be fully understood.

On the other hand, the commercialization of JPs presents exciting opportunities across industries, particularly in healthcare (*e.g.*, drug delivery and diagnostics), environmental applications (*e.g.*, water purification), and advanced materials (*e.g.*, smart coatings). As these sectors increasingly demand multifunctional materials with precise control over their properties, JPs are well-positioned to emerge as valuable options. However, to fully unlock their market potential, it is crucial to reduce production costs and prove their cost-effectiveness relative to existing materials. The economic success of JPs hinges heavily on their scalability. Additionally, with the growing focus on green chemistry and sustainable materials, JPs could be adapted for markets prioritizing environmentally friendly solutions.

Future research must adopt a multidisciplinary approach that merges experimental work with computational techniques, including machine learning, modeling, and simulation, to optimize JP design and expand their functionality. Computational tools can simulate complex reactions and predict how variations in parameters like monomer composition, reaction temperature, and surface functionalization impact JP structure and performance. Machine learning algorithms can also analyze vast experimental datasets to identify optimal synthesis pathways, accelerating the design process.

Although many applications of JPs have been explored in academic settings, much of the work remains in its early stages concerning practical commercial applications. A significant barrier lies in identifying the real-world challenges relevant to JP research, which requires researchers to collaborate across disciplines and broaden their expertise beyond particle synthesis. Ultimately, realizing the full potential of JPs demands a comprehensive approach that integrates both synthesis and application, as they are two sides of the same coin.

Author contributions

Yifan Li: contributed to the overall outline and writing of all sections of the manuscript. Fei Liu: wrote the sections on inorganic Janus nanoparticles and part of the hybrid nanoparticles section. Serkan Demirci: contributed to writing the sections on polymeric Janus nanoparticles. Utsav Kumar Dey: contributed to writing the sections on polymeric Janus nanoparticles. Thamer Rawah: contributed to writing the sections on polymeric Janus nanoparticles and produced some illustrations. Aneeba Chaudary: contributed to writing the sections on polymeric Janus nanoparticles. Ricardo Ortega: contributed to writing the sections on polymeric Janus nanoparticles and figure illustrations. Zhengtao Yang: contributed to writing the applications section on JPs. Emad Pirhadi: contributed to writing the sections on simulations. Bingrui Huang: contributed to proofreading and editing the entire manuscript. Xin Yong: wrote the sections on thermodynamic analysis, modeling, and simulations. Shan Jiang: structured the manuscript, wrote the introduction, and contributed to writing and revising all sections of the manuscript.

Data availability

No primary research results, software or code have been included and no new data were generated or analyzed as part of this review.

Conflicts of interest

Prof. Shan Jiang and Dr Yifan Li are the co-founders of a startup company with business interests in developing JPs for coating applications. These activities are supported by an Innovation Corps Grant from the National Science Foundation.

Acknowledgements

We acknowledge support from different funding agencies for our work on Janus particles, including Iowa State University for the Start-up Fund and 3M for the Non-tenured Faculty, Innovation Acceleration Fund by Iowa Board of Regents and State Economic Development & Industry Relations (EDIR), American Chemical Society Petroleum Research Fund under grant no. 60264-DNI7/56884-DNI9, NSF Partnerships for Innovation Technology Translation (PFI-TT) award under grants no. 2213976, NSF grant no. 1939362 and DoD through the Strategic Environmental Research & Development Program under project no. WP24-4176.

References

1 P.-G. de Gennes, *Angew. Chem., Int. Ed. Engl.*, 1992, **31**, 842–845.
2 A. Walther and A. H. E. Müller, *Soft Matter*, 2008, **4**, 663–668.
3 A. Walther and A. H. E. Müller, *Chem. Rev.*, 2013, **113**, 5194–5261.
4 J. Zhang, B. A. Grzybowski and S. Granick, *Langmuir*, 2017, **33**, 6964–6977.
5 S. Jiang, J. Yan, J. K. Whitmer, S. M. Anthony, E. Luijten and S. Granick, *Phys. Rev. Lett.*, 2014, **112**, 218301.
6 A. G. Vanakaras, *Langmuir*, 2006, **22**, 88–93.
7 A. Tagliabue, L. Izzo and M. Mella, *Langmuir*, 2016, **32**, 12934–12946.
8 F. Wurm and A. F. M. Kilbinger, *Angew. Chem., Int. Ed.*, 2009, **48**, 8412–8421.
9 P. Chen, Y. Yang, B. Dong, Z. Huang, G. Zhu, Y. Cao and L.-T. Yan, *Macromolecules*, 2017, **50**, 2078–2091.
10 Q. Yang and K. Loos, *Polym. Chem.*, 2017, **8**, 641–654.
11 Z.-W. Li, Z.-Y. Lu, Z.-Y. Sun and L.-J. An, *Soft Matter*, 2012, **8**, 6693–6697.
12 H. Su, C. A. Hurd Price, L. Jing, Q. Tian, J. Liu and K. Qian, *Mater. Today Bio*, 2019, **4**, 100033.
13 J. Hu, S. Zhou, Y. Sun, X. Fang and L. Wu, *Chem. Soc. Rev.*, 2012, **41**, 4356–4378.
14 Y. Liu, J. Hu, X. Yu, X. Xu, Y. Gao, H. Li and F. Liang, *J. Colloid Interface Sci.*, 2017, **490**, 357–364.
15 T. Yang, L. Wei, L. Jing, J. Liang, X. Zhang, M. Tang, M. J. Monteiro, Y. Chen, Y. Wang, S. Gu, D. Zhao, H. Yang, J. Liu and G. Q. M. Lu, *Angew. Chem., Int. Ed.*, 2017, **56**, 8459–8463.
16 B. Greydanus, D. K. Schwartz and J. W. Medlin, *ACS Appl. Mater. Interfaces*, 2020, **12**, 2338–2345.
17 W. Cao, R. Huang, W. Qi, R. Su and Z. He, *ACS Appl. Mater. Interfaces*, 2015, **7**, 465–473.
18 W. E. Uspal, *J. Chem. Phys.*, 2019, **150**, 114903.
19 Z. Wu, L. Li, T. Liao, X. Chen, W. Jiang, W. Luo, J. Yang and Z. Sun, *Nano Today*, 2018, **22**, 62–82.
20 M. Vafaeezadeh and W. R. Thiel, *Angew. Chem., Int. Ed.*, 2022, **61**, e202206403.
21 A. Kirillova, C. Schliebe, G. Stoychev, A. Jakob, H. Lang and A. Synytska, *ACS Appl. Mater. Interfaces*, 2015, **7**, 21218–21225.
22 Y. Zhou, Y. Yang, X. Deng, G. Zhang, Y. Zhang, C. Zhang, S. Shuang, Y. He and W. Sun, *Sens. Actuators, B*, 2018, **276**, 204–210.
23 A. Miyagawa, C. Ito, Y. Ueda, S. Nagatomo and K. Nakatani, *Anal. Chim. Acta*, 2024, **1318**, 342933.
24 Q. He, H. Vijayamohanan, J. Li and T. M. Swager, *J. Am. Chem. Soc.*, 2022, **144**, 5661–5667.
25 B. Jurado-Sánchez, S. Campuzano, J. M. Pingarrón and A. Escarpa, *Microchim. Acta*, 2021, **188**, 416.
26 Y. Yi, L. Sanchez, Y. Gao and Y. Yu, *Analyst*, 2016, **141**, 3526–3539.
27 S. Yang, P. J. Hricko, P.-H. Huang, S. Li, Y. Zhao, Y. Xie, F. Guo, L. Wang and T. J. Huang, *J. Mater. Chem. C*, 2014, **2**, 542–547.
28 B. Li, M. Wang, K. Chen, Z. Cheng, G. Chen and Z. Zhang, *Macromol. Rapid Commun.*, 2015, **36**, 1200–1204.
29 E. Dehghani, M. Salami-Kalajahi and H. Roghani-Mamaqani, *Colloids Surf., B*, 2018, **170**, 85–91.
30 H.-M. Ding and Y.-Q. Ma, *Nanoscale*, 2012, **4**, 1116–1122.
31 K.-H. Roh, D. C. Martin and J. Lahann, *Nat. Mater.*, 2005, **4**, 759–763.
32 W. Li, H. Dong, G. Tang, T. Ma and X. Cao, *RSC Adv.*, 2015, **5**, 23181–23188.
33 P. Sundararajan, J. Wang, L. A. Rosen, A. Procopio and K. Rosenberg, *Chem. Eng. Sci.*, 2018, **178**, 199–210.
34 Z.-Q. Feng, K. Yan, J. Li, X. Xu, T. Yuan, T. Wang and J. Zheng, *Mater. Sci. Eng., C*, 2019, **104**, 110001.
35 H. Xie, Z.-G. She, S. Wang, G. Sharma and J. W. Smith, *Langmuir*, 2012, **28**, 4459–4463.
36 L.-T.-C. Tran, S. Lesieur and V. Faivre, *Expert Opin. Drug Delivery*, 2014, **11**, 1061–1074.
37 P. Yánez-Sedeño, S. Campuzano and J. M. Pingarrón, *Appl. Mater. Today*, 2017, **9**, 276–288.
38 Y. Wu, X. Lin, Z. Wu, H. Möhwald and Q. He, *ACS Appl. Mater. Interfaces*, 2014, **6**, 10476–10481.
39 J. R. Gomez-Solano, A. Blokhuis and C. Bechinger, *Phys. Rev. Lett.*, 2016, **116**, 138301.
40 S. Samin and R. van Roij, *Phys. Rev. Lett.*, 2015, **115**, 188305.
41 X. Ma, S. Jang, M. N. Popescu, W. E. Uspal, A. Miguel-López, K. Hahn, D.-P. Kim and S. Sánchez, *ACS Nano*, 2016, **10**, 8751–8759.
42 A. M. Pourrahimi and M. Pumera, *Nanoscale*, 2018, **10**, 16398–16415.

43 X. Yu, S. Huang, K. Chen, Z. Zhou, X. Guo and L. Li, *Ind. Eng. Chem. Res.*, 2015, **54**, 2690–2696.
44 Y. Zhao, H. Gu, Z. Xie, H. C. Shum, B. Wang and Z. Gu, *J. Am. Chem. Soc.*, 2013, **135**, 54–57.
45 A. F. Demirörs, M. T. Akan, E. Poloni and A. R. Studart, *Soft Matter*, 2018, **14**, 4741–4749.
46 Y. Liu, J. Wang, Y. Shao, R. Deng, J. Zhu and Z. Yang, *Prog. Mater. Sci.*, 2022, **124**, 100888.
47 A. Kirillova, C. Marschelke and A. Synytska, *ACS Appl. Mater. Interfaces*, 2019, **11**, 9643–9671.
48 G. Agrawal and R. Agrawal, *ACS Appl. Nano Mater.*, 2019, **2**, 1738–1757.
49 T. C. Le, J. Zhai, W.-H. Chiu, P. A. Tran and N. Tran, *Int. J. Nanomed.*, 2019, **14**, 6749–6777.
50 F. Liang, C. Zhang and Z. Yang, *Adv. Mater.*, 2014, **26**, 6944–6949.
51 C. Zhang, F. Liang and Z. Yang, in *Soft, Hard, and Hybrid Janus Structures*, World Scientific, Europe, 2017, pp. 1–30, DOI: 10.1142/9781786343130_0001.
52 C. Tang, C. Zhang, J. Liu, X. Qu, J. Li and Z. Yang, *Macromolecules*, 2010, **43**, 5114–5120.
53 Y. Duan, X. Zhao, M. Sun and H. Hao, *Ind. Eng. Chem. Res.*, 2021, **60**, 1071–1095.
54 M. Pan, L. Yang, B. Guan, M. Lu, G. Zhong and L. Zhu, *Soft Matter*, 2011, **7**, 11187–11193.
55 X. Yu, Y. Sun, F. Liang, B. Jiang and Z. Yang, *Macromolecules*, 2019, **52**, 96–102.
56 T. S. Skelhon, Y. Chen and S. A. F. Bon, *Langmuir*, 2014, **30**, 13525–13532.
57 J. W. Kim, J. Cho, J. Cho, B. J. Park, Y.-J. Kim, K.-H. Choi and J. W. Kim, *Angew. Chem., Int. Ed.*, 2016, **55**, 4509–4513.
58 L. Hong, S. Jiang and S. Granick, *Langmuir*, 2006, **22**, 9495–9499.
59 A. Tsyrenova, M. Q. Farooq, S. M. Anthony, K. Mollaeian, Y. Li, F. Liu, K. Miller, J. Ren, J. L. Anderson and S. Jiang, *J. Phys. Chem. Lett.*, 2020, **11**, 9834–9841.
60 S. Jiang, Q. Chen, M. Tripathy, E. Luijten, K. S. Schweizer and S. Granick, *Adv. Mater.*, 2010, **22**, 1060–1071.
61 S. Jiang, M. J. Schultz, Q. Chen, J. S. Moore and S. Granick, *Langmuir*, 2008, **24**, 10073–10077.
62 A. Tsyrenova, K. Miller, J. Yan, E. Olson, S. M. Anthony and S. Jiang, *Langmuir*, 2019, **35**, 6106–6111.
63 S. Jiang and S. Granick, *J. Chem. Phys.*, 2007, **127**, 161102.
64 S. Granick, S. Jiang and Q. Chen, *Phys. Today*, 2009, **62**, 68–69.
65 E. Dehghani, F. Amani and M. Salami-Kalajahi, *Polym. Adv. Technol.*, 2020, **31**, 2999–3007.
66 Y. Lan, J. Choi, H. Li, Y. Jia, R. Huang, K. J. Stebe and D. Lee, *Ind. Eng. Chem. Res.*, 2019, **58**, 20961–20968.
67 W. Zhai, Y. Song, Z. Gao, J.-B. Fan and S. Wang, *Macromolecules*, 2019, **52**, 3237–3243.
68 C. Kaewsaneha, A. Bitar, P. Tangboriboonrat, D. Polpanich and A. Elaissari, *J. Colloid Interface Sci.*, 2014, **424**, 98–103.
69 D. Baah and T. Floyd-Smith, *Microfluid. Nanofluid.*, 2014, **17**, 431–455.
70 X.-H. Ge, J.-P. Huang, J.-H. Xu, J. Chen and G.-S. Luo, *Soft Matter*, 2016, **12**, 3425–3430.
71 Y. Lan, J. Wu, S. H. Han, S. Yadavali, D. Issadore, K. J. Stebe and D. Lee, *ACS Sustainable Chem. Eng.*, 2020, **8**, 17680–17686.
72 T. Nisisako, *Curr. Opin. Colloid Interface Sci.*, 2016, **25**, 1–12.
73 Z. Nie, W. Li, M. Seo, S. Xu and E. Kumacheva, *J. Am. Chem. Soc.*, 2006, **128**, 9408–9412.
74 S. Yang, F. Guo, B. Kiraly, X. Mao, M. Lu, K. W. Leong and T. J. Huang, *Lab Chip*, 2012, **12**, 2097–2102.
75 K. H. Ku, J. H. Ryu, J. Kim, H. Yun, C. Nam, J. M. Shin, Y. Kim, S. G. Jang, W. B. Lee and B. J. Kim, *Chem. Mater.*, 2018, **30**, 8669–8678.
76 J. Lee, K. H. Ku, J. Kim, Y. J. Lee, S. G. Jang and B. J. Kim, *J. Am. Chem. Soc.*, 2019, **141**, 15348–15355.
77 K. H. Ku, Y. Kim, G.-R. Yi, Y. S. Jung and B. J. Kim, *ACS Nano*, 2015, **9**, 11333–11341.
78 K. H. Ku, Y. J. Lee, G.-R. Yi, S. G. Jang, B. V. K. J. Schmidt, K. Liao, D. Klinger, C. J. Hawker and B. J. Kim, *Macromolecules*, 2017, **50**, 9276–9285.
79 R. Deng, H. Li, J. Zhu, B. Li, F. Liang, F. Jia, X. Qu and Z. Yang, *Macromolecules*, 2016, **49**, 1362–1368.
80 R. Deng, F. Liang, J. Zhu and Z. Yang, *Mater. Chem. Front.*, 2017, **1**, 431–443.
81 A. H. Gröschel, A. Walther, T. I. Löbling, J. Schmelz, A. Hanisch, H. Schmalz and A. H. E. Müller, *J. Am. Chem. Soc.*, 2012, **134**, 13850–13860.
82 R. Deng, F. Liang, X. Qu, Q. Wang, J. Zhu and Z. Yang, *Macromolecules*, 2015, **48**, 750–755.
83 Y. Zhang, H.-R. Liu and F.-W. Wang, *Colloid Polym. Sci.*, 2013, **291**, 2993–3003.
84 E. B. Mock and C. F. Zukoski, *Langmuir*, 2010, **26**, 13747–13750.
85 Z. Chu, B. Zhong, W. Zhou, P. Cui, J. Gu, B. Tian, O. S. Olasoju, X. Zhang and W. Sun, *Colloids Surf., A*, 2020, **603**, 125183.
86 A. Perro, F. Meunier, V. Schmitt and S. Ravaine, *Colloids Surf., A*, 2009, **332**, 57–62.
87 C. Wang, C. Xu, H. Zeng and S. Sun, *Adv. Mater.*, 2009, **21**, 3045–3052.
88 I. Schick, S. Lorenz, D. Gehrig, S. Tenzer, W. Storck, K. Fischer, D. Strand, F. Laquai and W. Tremel, *Beilstein J. Nanotechnol.*, 2014, **5**, 2346–2362.
89 G. Zheng, S. Mourdikoudis and Z. Zhang, *Small*, 2020, **16**, 2002588.
90 A. Chauhan, M. Rastogi, P. Scheier, C. Bowen, R. V. Kumar and R. Vaish, *Appl. Phys. Rev.*, 2018, **5**, 041111.
91 M. Ha, J.-H. Kim, M. You, Q. Li, C. Fan and J.-M. Nam, *Chem. Rev.*, 2019, **119**, 12208–12278.
92 Y. Lv, S. Duan and R. Wang, *Prog. Nat. Sci.: Mater. Int.*, 2020, **30**, 1–12.
93 J. Qiu, Q. N. Nguyen, Z. Lyu, Q. Wang and Y. Xia, *Adv. Mater.*, 2022, **34**, 2102591.
94 F. Liu, Y. Li, Y. Huang, A. Tsyrenova, K. Miller, L. Zhou, H. Qin and S. Jiang, *Nano Lett.*, 2020, **20**, 8773–8780.

95 F. Liu, S. Goyal, M. Forrester, T. Ma, K. Miller, Y. Mansoorieh, J. Henjum, L. Zhou, E. Cochran and S. Jiang, *Nano Lett.*, 2019, **19**, 1587–1594.
96 Z. Yang, J. Wei, Y. I. Sobolev and B. A. Grzybowski, *Nature*, 2018, **553**, 313–318.
97 D. Lu, S. Hou, S. Liu, Q. Xiong, Y. Chen and H. Duan, *J. Phys. Chem. C*, 2022, **126**, 14967–14975.
98 J. Reguera, T. Flora, N. Winckelmans, J. C. Rodríguez-Cabello and S. Bals, *Nanoscale Adv.*, 2020, **2**, 2525–2530.
99 D. H. Gu, W. Choi and J. S. Son, *JACS Au*, 2022, **2**, 2307–2315.
100 E. B. Mock, H. De Bruyn, B. S. Hawkett, R. G. Gilbert and C. F. Zukoski, *Langmuir*, 2006, **22**, 4037–4043.
101 S. Torza and S. G. Mason, *J. Colloid Interface Sci.*, 1970, **33**, 67–83.
102 J. A. Waters, *Colloids Surf., A*, 1994, **83**, 167–174.
103 Y.-C. Chen, V. Dimonie and M. S. El-Aasser, *J. Appl. Polym. Sci.*, 1991, **42**, 1049–1063.
104 D. C. Sundberg, A. P. Casassa, J. Pantazopoulos, M. R. Muscato, B. Kronberg and J. Berg, *J. Appl. Polym. Sci.*, 1990, **41**, 1425–1442.
105 Y. C. Chen, V. Dimonie and M. S. El-Aasser, *Macromolecules*, 1991, **24**, 3779–3787.
106 Y. G. Durant and D. C. Sundberg, *J. Appl. Polym. Sci.*, 1995, **58**, 1607–1618.
107 Y. G. J. Durant and J. Guillot, *Colloid Polym. Sci.*, 1993, **271**, 607–615.
108 C. L. Winzor and D. C. Sundberg, *Polymer*, 1992, **33**, 3797–3810.
109 H. R. Sheu, M. S. El-Aasser and J. W. Vanderhoff, *J. Polym. Sci., Part A: Polym. Chem.*, 1990, **28**, 629–651.
110 C. Wei, A. Plucinski, S. Nuasaen, A. Tripathi, P. Tangboriboonrat and K. Tauer, *Macromolecules*, 2017, **50**, 349–363.
111 H. Kim, J. Cho, J. Cho, B. J. Park and J. W. Kim, *ACS Appl. Mater. Interfaces*, 2018, **10**, 1408–1414.
112 F. Tu and D. Lee, *J. Am. Chem. Soc.*, 2014, **136**, 9999–10006.
113 J.-B. Fan, H. Liu, Y. Song, Z. Luo, Z. Lu and S. Wang, *Macromolecules*, 2018, **51**, 1591–1597.
114 J.-B. Fan, Y. Song, H. Liu, Z. Lu, F. Zhang, H. Liu, J. Meng, L. Gu, S. Wang and L. Jiang, *Sci. Adv.*, 2017, **3**, e1603203.
115 A. Perro, S. Reculusa, S. Ravaine, E. Bourgeat-Lami and E. Duguet, *J. Mater. Chem.*, 2005, **15**, 3745–3760.
116 J. Qiu, M. Xie, Z. Lyu, K. D. Gilroy, H. Liu and Y. Xia, *Nano Lett.*, 2019, **19**, 6703–6708.
117 A. Ohnuma, E. C. Cho, P. H. C. Camargo, L. Au, B. Ohtani and Y. Xia, *J. Am. Chem. Soc.*, 2009, **131**, 1352–1353.
118 V. Mihali and A. Honciuc, *Adv. Mater. Interfaces*, 2017, **4**, 1700914.
119 M. M. Rahman, F. Montagne, H. Fessi and A. Elaissari, *Soft Matter*, 2011, **7**, 1483–1490.
120 J. Ge, Y. Hu, T. Zhang and Y. Yin, *J. Am. Chem. Soc.*, 2007, **129**, 8974–8975.
121 J.-W. Kim and K.-D. Suh, *Polymer*, 2000, **41**, 6181–6188.
122 Y. Li, F. Liu, S. Chen, A. Tsyrenova, K. Miller, E. Olson, R. Mort, D. Palm, C. Xiang, X. Yong and S. Jiang, *Mater. Horiz.*, 2020, **7**, 2047–2055.
123 J.-W. Kim, R. J. Larsen and D. A. Weitz, *J. Am. Chem. Soc.*, 2006, **128**, 14374–14377.
124 Y. Li, S. Chen, S. Demirci, S. Qin, Z. Xu, E. Olson, F. Liu, D. Palm, X. Yong and S. Jiang, *J. Colloid Interface Sci.*, 2019, **543**, 34–42.
125 L. C. Bradley, K. J. Stebe and D. Lee, *J. Am. Chem. Soc.*, 2016, **138**, 11437–11440.
126 B. Peng, H. R. Vutukuri, A. van Blaaderen and A. Imhof, *J. Mater. Chem.*, 2012, **22**, 21893–21900.
127 E. Sokolovskaya, J. Yoon, A. C. Misra, S. Bräse and J. Lahann, *Macromol. Rapid Commun.*, 2013, **34**, 1554–1559.
128 M. Fallahi-Samberan, M. Salami-Kalajahi, E. Dehghani and F. Abbasi, *Microchem. J.*, 2019, **145**, 492–500.
129 T. Fujibayashi and M. Okubo, *Langmuir*, 2007, **23**, 7958–7962.
130 D. Wu and A. Honciuc, *ACS Appl. Nano Mater.*, 2018, **1**, 471–482.
131 S. Pradhan, L. Xu and S. Chen, *Adv. Funct. Mater.*, 2007, **17**, 2385–2392.
132 W.-H. Chen, F. Tu, L. C. Bradley and D. Lee, *Chem. Mater.*, 2017, **29**, 2685–2688.
133 H. S. C. Hamilton and L. C. Bradley, *Polym. Chem.*, 2020, **11**, 230–235.
134 L. J. Gonzalez-Ortiz and J. M. Asua, *Macromolecules*, 1995, **28**, 3135–3145.
135 L. J. González-Ortiz and J. M. Asua, *Macromolecules*, 1996, **29**, 383–389.
136 L. J. González-Ortiz and J. M. Asua, *Macromolecules*, 1996, **29**, 4520–4527.
137 O. J. Karlsson, J. M. Stubbs, R. H. Carrier and D. C. Sundberg, *Polym. React. Eng.*, 2003, **11**, 589–625.
138 J. Stubbs, R. Carrier and D. C. Sundberg, *Macromol. Theory Simul.*, 2008, **17**, 147–162.
139 S. Hamzehlou, J. R. Leiza and J. M. Asua, *Chem. Eng. J.*, 2016, **304**, 655–666.
140 Y. Duda and F. Vázquez, *Langmuir*, 2005, **21**, 1096–1102.
141 V. Herrera, Z. Palmillas, R. Pirri, Y. Reyes, J. R. Leiza and J. M. Asua, *Macromolecules*, 2010, **43**, 1356–1363.
142 Y. Reyes and J. M. Asua, *J. Polym. Sci., Part A: Polym. Chem.*, 2010, **48**, 2579–2583.
143 E. Akhmatskaya and J. M. Asua, *J. Polym. Sci., Part A: Polym. Chem.*, 2012, **50**, 1383–1393.
144 E. Akhmatskaya and J. M. Asua, *Colloid Polym. Sci.*, 2013, **291**, 87–98.
145 M. Nedyalkova, G. Russo, P. Loche and M. Lattuada, *J. Chem. Inf. Model.*, 2023, **63**, 7453–7463.
146 D. Wu, J. W. Chew and A. Honciuc, *Langmuir*, 2016, **32**, 6376–6386.
147 V. Mihali and A. Honciuc, *ACS Nano*, 2019, **13**, 3483–3491.
148 M. W. Issa, D. Calderon, O. Kamlet, S. Asaei, J. N. Renner and C. L. Wirth, *ACS Appl. Eng. Mater.*, 2023, **1**, 1983–1996.

149 S. Porter, A. Ghosh, C. H. Liu, D. Kunwar, C. Thompson, R. Alcala, D. P. Dean, J. T. Miller, A. DeLaRiva, H. Pham, E. Peterson, A. Brearley, J. Watt, E. A. Kyriakidou and A. K. Datye, *ACS Catal.*, 2023, **13**, 5456–5471.
150 T. Zhao, X. Zhu, C.-T. Hung, P. Wang, A. Elzatahry, A. A. Al-Khalaf, W. N. Hozzein, F. Zhang, X. Li and D. Zhao, *J. Am. Chem. Soc.*, 2018, **140**, 10009–10015.
151 Y. Zhou, F. Shen, S. Zhang, Q. Zhao, Z. Xu and H. Chen, *ACS Appl. Mater. Interfaces*, 2020, **12**, 29876–29882.
152 J. Wu, C. Feng, X. Ma, S. Liu, C. Zhang, J. Han, L. Wang and Y. Wang, *ACS Appl. Polym. Mater.*, 2024, **6**, 1740–1750.
153 A. Walther, M. Hoffmann and A. H. E. Müller, *Angew. Chem., Int. Ed.*, 2008, **47**, 711–714.
154 A. Lotierzo, B. W. Longbottom, W. H. Lee and S. A. F. Bon, *ACS Nano*, 2019, **13**, 399–407.
155 K. Lee, L. Zhang, Y. Yi, X. Wang and Y. Yu, *ACS Nano*, 2018, **12**, 3646–3657.
156 K. Lee and Y. Yu, *Langmuir*, 2018, **34**, 12387–12393.
157 L. Zhang, M. Zhang, L. Zhou, Q. Han, X. Chen, S. Li, L. Li, Z. Su and C. Wang, *Biomaterials*, 2018, **181**, 113–125.
158 J. Song, B. Wu, Z. Zhou, G. Zhu, Y. Liu, Z. Yang, L. Lin, G. Yu, F. Zhang, G. Zhang, H. Duan, G. D. Stucky and X. Chen, *Angew. Chem., Int. Ed.*, 2017, **56**, 8110–8114.
159 J. Song, L. Lin, Z. Yang, R. Zhu, Z. Zhou, Z.-W. Li, F. Wang, J. Chen, H. Yang and X. Chen, *J. Am. Chem. Soc.*, 2019, **141**, 8158–8170.
160 X. Lin, S. Liu, X. Zhang, R. Zhu, S. Chen, X. Chen, J. Song and H. Yang, *Angew. Chem., Int. Ed.*, 2020, **59**, 1682–1688.
161 L. Zhang, Y. Chen, Z. Li, L. Li, P. Saint-Cricq, C. Li, J. Lin, C. Wang, Z. Su and J. I. Zink, *Angew. Chem., Int. Ed.*, 2016, **55**, 2118–2121.
162 S.-H. Hu and X. Gao, *J. Am. Chem. Soc.*, 2010, **132**, 7234–7237.
163 A. Kirillova, L. Ionov, I. V. Roisman and A. Synytska, *Chem. Mater.*, 2016, **28**, 6995–7005.
164 S. Berger, L. Ionov and A. Synytska, *Adv. Funct. Mater.*, 2011, **21**, 2338–2344.
165 H. Zhao, F. Liang, X. Qu, Q. Wang and Z. Yang, *Macromolecules*, 2015, **48**, 700–706.
166 H. Yang, F. Liang, Y. Chen, Q. Wang, X. Qu and Z. Yang, *NPG Asia Mater.*, 2015, **7**, e176–e176.